



# Fickian and thermal diffusion coefficients of binary mixtures of isobutylbenzene and *n*-alkanes at different concentrations from the optical beam deflection technique

Cite as: J. Chem. Phys. 151, 024202 (2019); <https://doi.org/10.1063/1.5082963>

Submitted: 26 November 2018 . Accepted: 13 June 2019 . Published Online: 11 July 2019

 Filipe Arantes Furtado, and  Abbas Firoozabadi



View Online



Export Citation



CrossMark

## ARTICLES YOU MAY BE INTERESTED IN

Large plasmonic field enhancement on hydrogen-absorbing transition metals at lower frequencies: Implications for hydrogen storage, sensing, and nuclear fusion

Journal of Applied Physics **126**, 023102 (2019); <https://doi.org/10.1063/1.5091723>

Combined plasmon-resonance and photonic-jet effect in the THz wave scattering by dielectric rod decorated with graphene strip

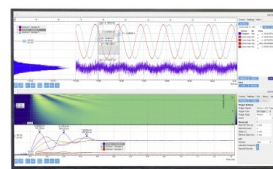
Journal of Applied Physics **126**, 023104 (2019); <https://doi.org/10.1063/1.5093674>

Counting quantum jumps: A summary and comparison of fixed-time and fluctuating-time statistics in electron transport

The Journal of Chemical Physics **151**, 034107 (2019); <https://doi.org/10.1063/1.5108518>

Challenge us.

What are your needs for  
periodic signal detection?



Zurich  
Instruments

# Fickian and thermal diffusion coefficients of binary mixtures of isobutylbenzene and *n*-alkanes at different concentrations from the optical beam deflection technique

Cite as: J. Chem. Phys. 151, 024202 (2019); doi: 10.1063/1.5082963

Submitted: 26 November 2018 • Accepted: 13 June 2019 •

Published Online: 11 July 2019



View Online



Export Citation



CrossMark

Filipe Arantes Furtado<sup>1,2,a)</sup>  and Abbas Firoozabadi<sup>1,3,b)</sup> 

## AFFILIATIONS

<sup>1</sup>Chemical Engineering Department, Yale University, 9 Hillhouse Avenue, New Haven, CT, 06511, United States

<sup>2</sup>Chemical Engineering Program - PEQ/COPPE, Federal University of Rio de Janeiro - UFRJ, Cidade Universitária, Rio de Janeiro - RJ, Brazil

<sup>3</sup>Reservoir Engineering Research Institute, Palo Alto, California 94301, USA

<sup>a)</sup>E-mail: [ffurtado@ufrj.br](mailto:ffurtado@ufrj.br)

<sup>b)</sup>E-mail: [af@rerinst.org](mailto:af@rerinst.org)

## ABSTRACT

We report the Fickian diffusion ( $D_{12}$ ), thermal diffusion ( $D_T$ ), and Soret ( $S_T$ ) coefficients of 4 binary mixtures of isobutylbenzene (IBB) and *n*-alkanes (*n*-hexane, *n*-octane, *n*-decane, and *n*-dodecane) at 298.15 K and atmospheric pressure. The concentration is varied in the whole range. The Optical Beam Deflection technique is used in the measurements. We first verify our measurements with published data. The concepts of molecular similarity and mobility are invoked to investigate  $D_{12}$  and  $D_T$  dependency on molecular weight and concentration. Our analysis reveals a combined effect of molecular mobility and similarity dependency of  $D_T$  on concentration and molecular weight of the *n*-alkanes. The mobility of individual molecules describes the  $D_{12}$  dependency on concentration and molecular weight of alkanes. The dependency of  $D_{12}$  on concentration weakens as the *n*-alkane molecular weight increases.  $D_T$  increases with IBB concentration for  $nC_6$  and  $nC_8$  and decreases with IBB concentration for  $nC_{10}$  and  $nC_{12}$ . In this work, we demonstrate that the temperature contrast factors can be accurately estimated without the use of an interferometer.

Published under license by AIP Publishing. <https://doi.org/10.1063/1.5082963>

## I. INTRODUCTION

When a fluid mixture is subjected to a temperature gradient, mass fluxes from Fickian diffusion and thermal diffusion occur in addition to energy flux. The segregation of species in a mixture under a temperature gradient was first observed in 1856 by Ludwig and later in 1880 by Soret. The thermal diffusion or Ludwig-Soret effect<sup>1,2</sup> has been introduced to describe the mass diffusion flux driven by a temperature gradient. Thermal diffusion creates a concentration gradient which is the driving force for the Fickian diffusion flux. When the system reaches the steady state, the Fickian and thermal diffusion fluxes balance each other, resulting in a zero net mass flux and a fully developed concentration gradient.<sup>3–5</sup>

The material diffusive flux ( $J_i$ ) of component *i* in a mixture of a given density ( $\rho$ ) under a temperature gradient can be described by the nonequilibrium thermodynamics theory.<sup>6,7</sup> In a two-component mixture, the multiplication of the thermal ( $D_T$ ) and Fickian ( $D_{12}$ ) diffusion coefficients by appropriate driving forces provides the flux of component 1 in a mixture of components 1 and 2,

$$J_1 = -\rho[D_{12}\nabla c_1 + c_1(1 - c_1)D_T\nabla T], \quad (1)$$

where  $c_1$  is the concentration in mass fraction of component 1 and  $T$  is the absolute temperature.

The first recognition of thermal diffusion was around 160 years ago; the phenomenon is, however, not fully understood.<sup>8</sup> The

challenges in the measurements of mixtures (with two or more components)<sup>9</sup> and the variety of molecular characteristics and interactions<sup>10</sup> have limited the understanding of the thermal diffusion phenomenon, especially for mixtures with more than two components. New measurements may provide a base for improved understanding of thermal diffusion and verification of theories.

Various reviews discuss the main experimental techniques and challenges in measuring Fickian and thermal diffusion coefficients.<sup>11–14</sup> The techniques include the Optical Beam Deflection (OBD), Thermal Gravitational Column (TGC), and Thermal Diffusion Forced Rayleigh Scattering (TDFRS). To examine various techniques, different laboratories<sup>15–20</sup> have measured 3 binary mixtures of *n*-dodecane (*n*C<sub>12</sub>), isobutylbenzene (IBB), and 1,2,3,4-tetracyclonaphthalene (THN) at 298.15 K and 0.5 mass fraction. These sets of mixtures are known as the Fontainebleau benchmark.<sup>15–20</sup> The data serve as a reliability test for experimental techniques in determination of the thermal diffusion coefficients. Compositional dependency of the Fontainebleau benchmark was published in 2013.<sup>21</sup>

Examples of application of thermal diffusion include the fractionation of bacteria,<sup>22</sup> characterization and separation of polymer solutions,<sup>23,24</sup> and spatial variation of various chemical species in subsurface formations.<sup>25,26</sup>

Hydrocarbon fluids in the subsurface are a complex mixture of organic components (e.g., alkanes, alkenes, and aromatic compounds of different molecule sizes and shapes). Aromatic compounds may contain multiple aromatic rings and heteroatoms such as nitrogen, sulfur, and oxygen. An example of the strong effect of thermal diffusion on the segregation of hydrocarbons is the Yufutsu gas field (Japan).<sup>27</sup> Because of the geothermal gradient, the Yufutsu field had a fluid with the heavier components atop of the lighter phase. Ghorayeb *et al.*<sup>27,28</sup> modeled the species distribution in the Yufutsu field based on thermal diffusion. They predict the observed upside-down behavior. The study by Ghorayeb *et al.*<sup>27,28</sup> reveals that thermal diffusion can vastly influence the distribution of components in hydrocarbon formations.

In the last few years, several authors have studied the relation between thermal diffusion coefficients and physical properties. Blanco *et al.*<sup>29</sup> report on the correlation of  $D_T$  of *n*-alkane-*n*-alkane liquid mixtures and molecular weight (MW), viscosity, and thermal expansion coefficient. Madariaga *et al.*<sup>30</sup> have studied the composition dependency of  $D_T$  in the *n*-alkane-*n*-alkane mixtures and observe that  $D_T$  is proportional to molecular weight difference between the mixture constituents and to the ratio of thermal expansion coefficient and viscosity of the mixture. A linear dependency of  $D_T$  with concentration has been observed. de Mezquia *et al.*<sup>31</sup> have shown that  $S_T$  in equimolar *n*-alkane mixtures has a trend similar to isotopiclike mixtures, which depends on the molecular weight difference between the *n*-alkanes. They suggest a correlation between  $S_T$  and the pure component properties (viscosity and thermal expansion coefficient) and the density of the equimolar mixture, allowing a quantitative prediction at different concentrations. Molecular dynamics simulations have been used to calculate  $S_T$  of the *n*-alkane-*n*-alkane binary mixtures. Perronace *et al.*<sup>32</sup> have simulated *n*-pentane-*n*-decane mixtures at different concentrations to obtain the Soret coefficients; they have compared the results to measured data. The difference is less than 35% for the boundary driven nonequilibrium molecular dynamics method (BD-NEMD). Furtado

*et al.*<sup>33</sup> have also performed molecular dynamics simulations using the BD-NEMD method and have computed  $S_T$  of the *n*-pentane-*n*-decane mixture at 0.5 mole fraction; they found deviations ranging from 17.5% to 37%.

Polyakov *et al.*,<sup>34</sup> Hashmi *et al.*,<sup>35</sup> and Larrañaga *et al.*<sup>36</sup> have recently reported measured thermal and Fickian diffusion coefficients of binary mixtures consisting of an aromatic and an *n*-alkane species. Polyakov *et al.*<sup>34</sup> have measured the Soret coefficients for mixtures of *n*-alkanes and benzene and branched alkanes and benzene. They have observed the effect of branching in  $S_T$  is more pronounced than the effect of the molecular weight. Hashmi *et al.*<sup>35</sup> have studied thermal diffusion and Fickian diffusion coefficients of multiringed aromatics (naphthalene, phenanthrene, pyrene, and coronene) diluted in *n*-alkanes (*n*-hexane, *n*-decane, and *n*-hexadecane). They show the variation of thermal diffusion coefficients with the number of aromatic rings. The multiringed molecules were intended to represent asphaltene molecules. Larrañaga *et al.*<sup>36</sup> investigate thermal diffusion in mixtures of toluene (tol) and *n*-alkane, and 1-methylnaphthalene (MN) and *n*-alkane as a function of concentration at 25 °C. They observe that  $D_T$  varies linearly with concentration in the binary *n*-alkane-aromatic mixtures; the linear variation allows for calculations based on infinite dilution.

An extensive set of  $S_T$  measurements in 41 binary equimolar mixtures (among 10 different organic compounds) have been reported by Hartmann *et al.*<sup>37</sup> The authors have found an additive rule for the heat of transports in equimolar mixtures. They assign a single value to the heat of transport of each substance. They show the heat of transport of a given component in an equimolar mixture is a property of the pure component. Since only differences between heats of transport can be experimentally determined, Hartmann *et al.*<sup>37</sup> choose a reference component to calculate the single component heat of transport. They chose tetralin as the reference and assigned a value of zero for its heat of transport. The thermophobicity was then defined as the heat of transport of the single component with respect to the heat of transport of tetralin. Using the values of thermophobicities, they calculate  $S_T$  for the equimolar mixtures and organized the components with respect to the tendency to segregate to the cold side. The higher the thermophobicity, the higher is the tendency to segregate to the cold side. Hartmann *et al.*<sup>37</sup> discuss their results using the thermodiffusion theory developed by Morozov.<sup>38</sup> Later, Hartmann *et al.*<sup>39</sup> extended the number of components in their analysis from 10 to 23. They studied 77 out of 253 possible combinations of the pure components in binary equimolar mixtures. The thermophobicity was evaluated for the larger set of mixtures, and no significant variation was found with the thermophobicities of the first ten components (1-methylnaphthalene was the only exception). Their results indicate that the thermophobicity is a property of the pure component in equimolar mixtures. Hartmann *et al.*<sup>39</sup> examined the composition dependence of 22 binary mixtures using the theory of Morozov;<sup>38</sup> the composition dependency was modeled by the excess volume of mixing.

In this work, we use the Optical Beam Deflection (OBD) technique<sup>21,40,41</sup> to determine the Fickian Diffusion ( $D_{12}$ ), thermal diffusion ( $D_T$ ), and Soret ( $S_T$ ) coefficients of binary mixtures of two molecules of different shapes (i.e., one aromatic and one *n*-alkane). The apparatus is modified from the one reported by Hashmi *et al.*

(2016).<sup>35</sup> We investigate mixtures of an *n*-alkane (*n*-hexane, *n*-octane, *n*-decane, and *n*-dodecane) and isobutylbenzene at 25 °C and 1 atm at five different concentrations. The motivation of this work is to evaluate the composition effect and the influence of molecular chain length of the *n*-alkanes in Fickian diffusion and thermal diffusion coefficients. We invoke the concepts of mobility and similarity of molecules to analyze the influence of molecular size and shape. To the best of our knowledge, this is the first report of the binary systems of isobutylbenzene (IBB) and *n*-hexane ( $nC_6$ ), *n*-octane ( $nC_8$ ) and *n*-decane ( $nC_{10}$ ) in the entire composition range. We validate the setup by verifying our results for mixtures of toluene and  $nC_6$ , and IBB (isobutylbenzene) and  $nC_{12}$  with literature data.

The measurement of Fickian and thermal diffusion coefficients by the Optical Beam Deflection (OBD) requires the derivatives of refractive index with composition  $(\partial n/\partial c_1)_{P,T}$  and temperature  $(\partial n/\partial T)_{P,c}$ . These two optical properties,  $(\partial n/\partial c_1)_{P,T}$  and  $(\partial n/\partial T)_{P,c}$ , are commonly determined by independent experiments using, respectively, a refractometer (accuracy of  $10^{-4}$ ) and an interferometer (accuracy in the order of  $10^{-6} \text{ K}^{-1}$ ). In this work, we determine  $(\partial n/\partial c_1)_{P,T}$  using a refractometer, while  $(\partial n/\partial T)_{P,c}$  is estimated based on deflection of the laser beam. We consider  $(\partial n/\partial T)_{P,c}$  as a parameter to be estimated together with  $D_{12}$  and  $D_T$ , similar to Königer *et al.*<sup>42</sup> and Kolodner *et al.*<sup>43</sup> Our calculation procedure is different. We compare our estimated  $(\partial n/\partial T)_{P,c}$  to the literature data to demonstrate agreement.

## II. EXPERIMENTAL

### A. Materials and sample preparation

The *n*-alkanes in this work include *n*-hexane ( $nC_6$ ), *n*-octane ( $nC_8$ ), *n*-decane ( $nC_{10}$ ), and *n*-dodecane ( $nC_{12}$ ). They are from Acros Organics ( $nC_6$ ,  $nC_8$ , and  $nC_{10}$ —purity higher than 99%) and Alfa Aesar ( $nC_{12}$ —purity higher than 99%). The toluene (tol) is from Baker with purity higher than 99.5%, and isobutylbenzene (IBB) is from Aldrich with purity higher than 99%. All chemicals are used without further purification.

The mixtures (see Table I) are prepared from weighing the components by an analytical balance with a resolution of  $10^{-4}$  g. The components are mixed in a cleaned vial starting by the less volatile component to eliminate evaporation. Subsequently, the vial containing the mixture is stirred to attain homogeneity.

### B. Optical beam deflection setup

The Optical Beam Deflection apparatus is a modification of the setup by Hashmi *et al.*<sup>35</sup> The changes include a new cell with a square

**TABLE I.** Binary mixtures of toluene(tol)-*n*-alkane( $nC_i$ ) and isobutylbenzene(IBB)-*n*-alkane( $nC_i$ ) at different concentrations of toluene and isobutylbenzene ( $c_1$ ).

System	$c_1$ (mass fraction)				
tol- $nC_6$	...	0.262	0.517	0.762	0.953
IBB- $nC_6$	0.100	0.300	0.500	0.700	0.900
IBB- $nC_8$	0.100	0.300	0.500	0.700	0.900
IBB- $nC_{10}$	0.100	0.300	0.500	0.700	0.900
IBB- $nC_{12}$	0.100	0.300	0.500	0.700	0.900

glass piece (instead of a circular shape) and an electrically heating/cooling system using peltier modules. Another improvement is the optimization of the cell size to allow a more homogeneous temperature distribution over the entire copper plates. Additional improvements are made in the electronics and programming to allow the setup to work with the new configuration. A schematic of the Optical Beam Deflection (OBD) apparatus is shown in Figs. 1 and 2. The entire apparatus is assembled on an optical table with active compressed air actuators to ensure a vibration-free environment. The setup consists of a squared glass frame of optical quality with an optical path length of 25.0 mm, wall thickness of 2.5 mm, and height of 4.0 mm. The glass frame is sandwiched between two copper plates ( $60.0 \times 75.0 \times 12.5 \text{ mm}^3$ ) with milled grooves that fit the optical glass piece. The glass-copper sealing is by squared cross section Viton o-rings. The parts in contact with the o-rings (glass ends and copper) are well polished (glass was optically polished) to prevent leakage and formation of gas bubbles. The gap size ( $h$ ) between the plates is  $1.771 \pm 0.006 \text{ mm}$ , measured by precision spacers. The parallel spacing of plates and gap size are confirmed by a telemicroscope (Gaertner) to a maximum error of  $\pm 0.006 \text{ mm}$  at the cell ends. The copper plates can be independently heated or cooled by two separate peltier modules of  $50 \times 50 \text{ mm}^2$  (Custom Thermoelectric 12711-9L31-06CW— $P_{max}$  of 51 W and  $I_{max}$  of 6.0 A). Each peltier module has one side in thermal contact with the copper plates and the other side with a water heat exchanger fed by a temperature-controlled water bath. The use of H-bridge amplifiers (FTX300) together with an arduino microcontroller allows the inversion of electric current and voltage control applied to the peltiers. Precision negative temperature coefficient (NTC) thermistors (Measurement Specialties 46 037) are inserted in drilled holes in each plate to measure the temperature. High precision in the measured resistance of the thermistors is achieved using a custom-built Wheatstone bridge and one signal amplifier (Tacuna) for each thermistor, providing a temperature resolution of 0.1 mK. The NTC thermistors were calibrated by a third calibrated NTC thermistor

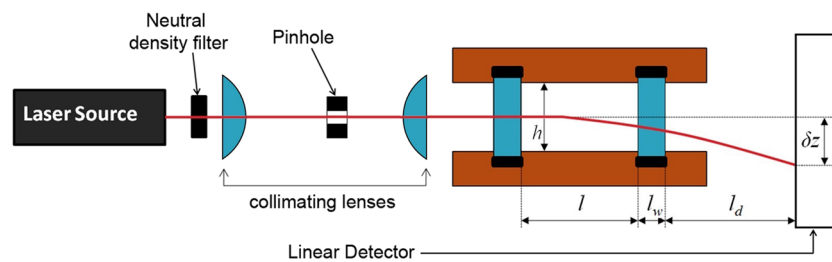


**FIG. 1.** Schematic of the optical beam deflection setup.

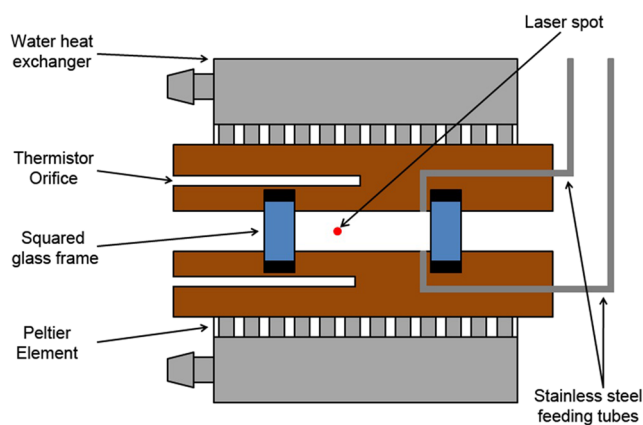


FIG. 2. Sketch of the optical beam deflection cell.

with an accuracy of  $0.1^\circ\text{C}$ , the same absolute accuracy as in temperature measurements by Königer.<sup>44</sup> We have observed a maximum deviation around 2 mK in the calibration range ( $23\text{--}28^\circ\text{C}$ ) when both thermistors are used to measure the temperature of a copper block. The temperature control is established by independent control of each peltier module using a closed loop proportional integral derivative (PID) controller programmed in LabView. The cell is assembled using 4 bolts in its body, while the peltier modules and water heat exchangers are clamped to the entire cell using custom built aluminum clampers. The cell is filled with the liquid mixture through stainless steel tubing using a gas tight syringe. Visual inspection guarantees absence of gas bubbles inside the cell. The setup is aligned using a calibrated height gage with a precision of 0.02 mm.

A 7-mW He-Ne laser (JDSU 1137P, wavelength of 632.8 nm) is used as the light source; its power is reduced by a neutral density filter (optical density of 2.0) to avoid local heating of the liquid sample. Two plano-convex lenses (focal distance of the first and second lens, respectively, 300 and 100 mm) are mounted on a telescope arrangement with a common focal plane to collimate the laser beam and reduce the laser spot. An iris pin hole (minimum aperture of 0.8 mm) is used to remove stray light from the collimation process. The collimated laser beam enters parallel to the cell's plates in the middle of the vertical gap between the plates. After passing through the glass containing the liquid mixture, the laser beam position is detected by a calibrated linear position sensor (UDT Instruments—model 1239), 504 cm away from the exit glass window of the cell. The detector is connected to an optical position indicator (UDT Instruments—model 431). A blackout rubberized fabric is used to provide a complete dark environment for the setup, blocking light coming from other sources.

All signals generated by the setup (i.e., temperature and laser position signals) are sent to a data acquisition system (NI cDAQ with appropriate cards for reading and generating analogical signals—National Instruments) and interpreted in the LabView software, recorded at a frequency of around 2 Hz.

A typical OBD experiment is conducted in two main steps after alignment of the laser and the setup. First, the cell is loaded with

the liquid mixture. The top and bottom plates are maintained at the same temperature for a period of time, long enough for the liquid mixture to become completely mixed (equilibrium is reached). In the next step, the temperatures of the top and bottom plates are brought to the desired values to subject the fluid system to a known temperature gradient. The choice of which plate should be heated and cooled is made to avoid convection in the fluid mixture. If the Soret coefficient is positive for the denser component, heating of the mixture from above will produce a convection-free pure diffusive state.<sup>45–47</sup> We have heated all the mixtures from the top plate since the Soret coefficient  $S_T$  for the denser components (IBB and Toluene) is positive. To apply the temperature gradient, both top and bottom temperatures are, respectively, changed by  $+\Delta T/2$  and  $-\Delta T/2$  ( $\Delta T$  is the desired temperature difference). The applied temperature differences ( $\Delta T$ ) are  $1.0\text{--}1.5^\circ\text{C}$  in different experiments. Initially when applying the temperature gradient, the laser beam experiences a fast and pronounced deflection due to the refractive index gradient  $dn/dz$  arising from the temperature gradient. The early deflection is a strong function of  $(\partial n/\partial T)_{P,c}$  and the thermal diffusivity  $\alpha$  of the mixture. In our apparatus, the steady state temperature of each copper plate is reached in about 120 s after the start of heating and cooling processes. A temperature overshoot in both plates is observed before the steady state temperature is established. This leads to a fast deflection of the laser beam. The segregation of the components along the height of the cell is a slow process. The laser deflection  $\delta z$  is proportional to the refractive index gradient (from temperature and concentration gradients) and to the characteristic lengths of the setup,<sup>40,41,43</sup>

$$\delta z = l \frac{dn}{dz} \left( \frac{l}{2n} + \frac{l_w}{n_w} + \frac{l_d}{n_{air}} \right), \quad (2)$$

where  $n$ ,  $n_w$ , and  $n_{air}$  are, respectively, the refractive indices of the liquid mixture, optical glass frame, and air;  $l$ ,  $l_w$ , and  $l_d$  are, respectively, the distance of the optical path in the liquid, glass wall, and the distance from the glass exit to the detector. The vertical refractive index gradient in a binary mixture is related to the vertical temperature and concentration gradients,

$$\frac{dn}{dz} = \frac{dc_1}{dz} \left( \frac{\partial n}{\partial c_1} \right)_{P,T} + \frac{dT}{dz} \left( \frac{\partial n}{\partial T} \right)_{P,c_1}, \quad (3)$$

where  $(\partial n/\partial c_1)_{P,T}$  and  $(\partial n/\partial T)_{P,c}$  are the contrast factors of concentration and temperature and  $c_1$  is the concentration of component 1 in mass fraction. The vertical temperature and concentration gradients are computed from the numerical solution of the energy balance expression [Eq. (4) below] and diffusion mass transport expression [Eq. (5) below]. The time dependent temperatures at the liquid-copper interfaces and the assumption of zero mass flux at the walls are the boundary conditions. The energy and mass balance expressions are given by, respectively,

$$\frac{\partial T}{\partial t} = \alpha \nabla^2 T, \quad (4)$$

and

$$\frac{\partial c}{\partial t} = D_{12} \nabla^2 c_1 + c_1(1 - c_1) D_T \nabla^2 T. \quad (5)$$

In Eq. (4),  $\alpha$  is the thermal diffusivity of the mixture, calculated using the thermal conductivity, density, and heat capacity of the mixtures in the Fillipov equation in the work of Poling *et al.*<sup>48</sup> The density and heat capacity of the mixtures are assumed to be a linear function of the pure component properties and composition. The pure component properties (thermal conductivity, density, and heat capacity) of the mixture constituents are from the literature.<sup>49–52</sup>

The Soret coefficient ( $S_T$ ) in a binary mixture is given by the ratio of the thermal diffusion coefficient ( $D_T$ ) to the Fickian diffusion coefficient ( $D_{12}$ ),

$$S_T = \frac{D_T}{D_{12}}. \quad (6)$$

The measured data are the laser deflection, temperatures of both plates, overall concentration of the mixture (in mass fraction), concentration contrast factor, and characteristic lengths of the setup. The solution of Eqs. (2)–(5) can provide  $D_{12}$ ,  $D_T$ , and the temperature contrast factor to be discussed in Sec. II D. Each deflection experiment is repeated 7–10 times for each of the 24 mixtures, totaling around 200 deflection plots.

### C. Optical property measurement

The refractive index of mixtures is measured using an Atago refractometer (RX-5000a) with a resolution of  $10^{-5}$ , repeatability of  $4 \times 10^{-5}$ , and temperature control accuracy of  $\pm 0.05$  °C. The refractometer operates at a wavelength of 589.3 nm, approximating the sodium D-line. The laser source in our experiments has a wavelength of 632.8 nm. de Mezquia *et al.*,<sup>4</sup> referring to the work of Sechenyh *et al.*<sup>53</sup> and Camerini-Otero *et al.*,<sup>54</sup> discuss the error in  $(\partial n/\partial c_1)_{P,T}$  due to the wavelength difference between the refractometer and the laser source in the OBD setup of  $\sim 44$  nm may be around 0.5%–1%. This difference results in a small error in  $D_{12}$ ,  $D_T$ , and  $S_T$ .

The concentration contrast factor  $(\partial n/\partial c_1)_{P,T}$  is estimated from a polynomial (cubic in concentration) of measured refractive index at different concentrations at 25 °C. We measured the refractive index at 13 different concentrations (mass fractions) varying from 0 to 1 for each mixture. At least 8 repetitions for each data point are conducted.

The temperature contrast factor  $(\partial n/\partial T)_{P,c}$  is computed as a parameter from the numerical solution of Eqs. (2)–(5) using the beam deflection data from OBD experiments. Königer *et al.*<sup>42</sup> and Kolodner *et al.*<sup>43</sup> also demonstrate that  $(\partial n/\partial T)_{P,c}$  can be estimated as a parameter based on beam deflection data and solution of Eqs. (2)–(5). An interferometer can be used to independently determine the contrast factors (error in the order of  $10^{-6}$ ).<sup>21,42,55</sup> Königer *et al.*<sup>42</sup> estimated one of the two contrast factors  $(\partial n/\partial T)_{P,c}$  in a two-color OBD experiment as a fitting parameter, while the other is determined interferometrically. The determination of thermal diffusion coefficients in OBD experiments is based on the  $N - 1$  beams ( $N$  is the number of components).<sup>9</sup> Königer *et al.*<sup>42</sup> report that in ternary mixtures, a slight error in the ratio between the two contrast factors  $(\partial n/\partial T)_{P,c}$  introduces a large error in the measured thermal diffusion coefficients. The authors report the difference between the interferometrically measured  $(\partial n/\partial T)_{P,c}$  and one based on the laser beam deflection to be around 0.1%.

The difference between the methodology in this work and the method by Kolodner *et al.*<sup>43</sup> is in the mathematical approach used to estimate the desired parameters, to be explained in Sec. II D. Our methodology is based on:

- (1) The pronounced initial beam deflection from the contribution of  $(\partial n/\partial T)_{P,c}$  and thermal diffusivity ( $\alpha$ ) of the mixture;
- (2) The fluctuations in the beam position at steady state (fully developed concentration and temperature gradients) from temperature fluctuations as observed by Zhang *et al.*<sup>40</sup>

The initial beam deflection and beam position fluctuation at steady state are related to the heat diffusion time [ $\tau_T$  – Eq. (7) below], which is about 25–80 times shorter than the mass diffusion time [ $\tau_D$  – Eq. (8) below] for our system,

$$\tau_T = \frac{h^2}{\pi^2 \alpha}, \quad (7)$$

$$\tau_D = \frac{h^2}{\pi^2 D_{12}}. \quad (8)$$

Based on  $\alpha$  and the measured temperature of the thermistors, we can calculate the transient temperature distribution along the height of the cell from the solution of the energy equation. At the beginning of an experiment, the heat and mass diffusion processes can be considered decoupled based on a small Lewis number<sup>43</sup> (defined by Kolodner<sup>43</sup> as  $L = D_{12}/\alpha$  or  $L = \tau_T/\tau_D$ ) of the order of  $10^{-2}$ . The transient temperature distribution during the initial laser deflection is used to estimate  $(\partial n/\partial T)_{P,c}$ . The accuracy is improved by using the fluctuations in laser deflection at steady state (i.e., fully developed concentration and temperature gradients). At steady state, the laser position fluctuations are from temperature fluctuations<sup>40</sup> as supported by a small Lewis number.

Kolodner *et al.*<sup>43</sup> use a cell with a gap size of  $h = 3.0$  mm. In our work,  $h = 1.771$  mm. This difference in  $h$  results in shorter mass and heat diffusion times in our setup. A smaller gap reduces the time for an experiment.

During the heating/cooling stage of an OBD experiment from electric heating, the temperatures of the plates cannot be switched instantaneously to desired values. The time to fully establish a desired temperature gradient in the liquid is a function of the peltier heating rate and the thermal diffusivity of the liquid. The heating rate affects the coupled temperature and concentration gradients. Based on the expression for the mass diffusion time [Eq. (8)], one can show that a smaller gap will generate a faster mass diffusion time. A small gap would fulfill the Rayleigh number conditions to avoid convection.<sup>45–47</sup> If the plate heating rate is low and the gap is small, the time it takes to develop the desired temperature gradient in the liquid will depend more on the time to bring the plates to the experimental temperature than on the thermal diffusivity of the liquid. In this case, a significant concentration gradient may develop in the transient temperature period. Consequently, the laser beam will be also deflected due to a concentration gradient (function of time) before the desired temperature gradient in the liquid is established. At a constant heating rate, a decrease in  $h$  leads to shorter diffusion time and increase the coupling.

Based on the statements 1 and 2 of our methodology and the support from the Lewis number, one can employ the solution

scheme we have used to determine  $D_{12}$ ,  $D_T$ , and  $(\partial n/\partial T)_{P,c}$  and also decouple the concentration and temperature contributions to the total beam deflection.

The high accuracy of our methodology is demonstrated by a comparison of the computed  $(\partial n/\partial T)_{P,c}$  for mixtures of IBB- $nC_{12}$  and tol- $nC_6$  with the literature measurements.

## D. Parameter estimation

The solution of Eqs. (2)–(5) provides  $D_{12}$ ,  $D_T$ , and  $(\partial n/\partial T)_{P,c}$ . In the physical setup, the thermistors are positioned 7 mm above the copper-liquid interface, and consequently, the measured temperature is slightly different from that of the copper-liquid interface. To determine the temperature at the copper-liquid interface, the energy equation [Eq. (4)] is solved numerically in the domain consisting of top copper plate, liquid mixture, and bottom copper plate. The boundary conditions are the temperatures measured by thermistors in the copper plates (i.e., temperatures 7 mm above and below the liquid-copper interfaces) and the equality of heat flux between copper and liquid interface. The thermistors' response time is also considered in the solution.

After the computation of the copper-liquid interface temperature, Eqs. (4) and (5) together with Eqs. (2) and (3) are solved numerically in the liquid domain. We first examined a deterministic method (Gauss-Newton) to determine  $D_{12}$ ,  $D_T$ , and  $(\partial n/\partial T)_{P,c}$ , which proved unsuccessful due to convergence issues. Usually, the deterministic methods require a good enough initial guess. In our problem, the initial guesses we used had convergence issues. We then adopted a stochastic method to obtain good enough initial guesses for the deterministic method. We employ the particle swarm optimization methodology<sup>56</sup> based on implementation of Schwaab *et al.*,<sup>57</sup> Schwaab and Pinto,<sup>58</sup> and Ourique *et al.*<sup>59</sup> as the stochastic method for the nonlinear parameter estimation.

Integration of the discretized form of Eqs. (3)–(5) was accomplished using the DASSL (Differential Algebraic System Solver).<sup>60</sup>

The estimations are carried out 2 times for each deflection data set. All computations are performed in a cluster of computers.

## E. Mobility and similarity

In Refs. 61 and 62, two effects, (1) mobility of each individual component and (2) similarity of the two species, have been found to be related to thermal diffusion in binary liquid mixtures.

The mobility is related to free movement of a molecule in a medium. An increase in mobility is from the increase in the velocity of that molecule in the medium. Mobility is then associated with the self-molecular diffusion coefficient  $D_i$  (for pure a component) or to the tracer diffusion coefficient  $D_i^*$  (self-diffusion of a molecule in a mixture). The mobility of an individual component is related to its Brownian motion.<sup>6,61–64</sup> In a mixture, mobility varies inversely with mixture viscosity and directly with the tracer diffusion coefficient. In a pure component, mobility varies inversely with the component viscosity and directly with self-molecular diffusion coefficient.<sup>5,61,62</sup> When the viscosity of a mixture increases, it will impede the movement of the molecule, which will lead to a reduction in the molecule velocity and thus, in mobility and tracer diffusion coefficient. In pure  $n$ -alkanes, there is an inverse relation between mobility and  $n$ -alkane chain length. An increase in the  $n$ -alkane chain length

(i.e., an increase in molecular weight) reduces the self-molecular diffusion coefficient<sup>65</sup> and increases its dynamic viscosity and thus decreases mobility.<sup>5,61,62</sup>

The tracer diffusion coefficient ( $D_i^*$ ) is a function of composition such as the molecular diffusion coefficient ( $D_{12}$ ).<sup>48</sup> When the concentration of species  $i$  tends to zero, ( $c_i \rightarrow 0$ ),  $D_i^*$  tends to the infinite dilution diffusion coefficient in the solvent  $j$  ( $D_{ij}^\circ$ ).<sup>47</sup> On the other hand, when  $c_i \rightarrow 1.0$ ,  $D_i^* \rightarrow D_i$ .<sup>48</sup> Then,  $D_i$  or  $D_i^*$  (or even  $D_{ij}^\circ$ ) can be a good choice to quantify mobility. However, measurement of  $D_i$  or  $D_i^*$  is more complex than the measurement of  $D_{12}$ , and other properties may be preferred to quantify mobility. The models developed by Darken<sup>66,67</sup> and Vignes<sup>68</sup> relate the Maxwell-Stefan diffusion coefficient ( $\mathcal{D}_{12}$ ) to, respectively,  $D_i^*$  and  $D_{ij}^\circ$ . Based on the model by Vignes,<sup>68</sup> the plot of  $\log(\mathcal{D}_{12})$  vs mole fraction is linear for mixtures that do not strongly associate. The implication is that  $\mathcal{D}_{12}$  is a function of  $D_{ij}^\circ$ , indicating that the Maxwell-Stefan diffusion coefficient ( $\mathcal{D}_{12}$ ) can be used as a measure of mobility. In fact,  $\mathcal{D}_{12}$  is proportional to mobility ( $\mathcal{D}_{12}$  increase as mobility increases), as pointed out by Leahy-Dios *et al.*<sup>62</sup> An increase in mobility also increases  $\mathcal{D}_{12}$ .

Several authors<sup>6,29,61–63</sup> use other properties to quantify mobility. Blanco *et al.*<sup>29</sup> quantify mobility as the inverse of mixture dynamic viscosity. A higher mixture viscosity lower molecules velocity and reduces  $D_i^*$  and  $D_{12}$ . Tyrrel and Harris<sup>63</sup> equate the Onsager coefficients to the mobility (or mobility coefficients). de Groot and Mazur<sup>6</sup> relate mobility to diffusion coefficients through a generalized Fokker-Einstein equation. The mobilities defined in the Fokker-Einstein equation have a dimension of velocity per unit force on a mole (or molecule). de Groot and Mazur<sup>6</sup> also found a relation between mobility and the Onsager coefficients. Onsager coefficients are functions of the transport properties of mixtures, including the diffusion coefficients. Leahy-Dios and Firoozabadi<sup>61</sup> use the physical properties that influence mobility of pure components to interpret  $D_{12}$  in equimass mixtures of  $nC_{10}$ - $nC_i$  and 1-methylnaphthalene- $nC_i$ . They find indications that  $D_{12}$  can be described solely by mobility. Leahy-Dios *et al.*<sup>62</sup> use the fact that mobility and Maxwell-Stefan diffusion coefficient ( $\mathcal{D}_{12}$ ) are proportional ( $\mathcal{D}_{12}$  increases as mobility increases) and interpret  $\mathcal{D}_{12}$  as a measure of mobility. The Stokes-Einstein equation [Eq. (9) below] is defined for the diffusion of spherical molecules in a dilute solution.<sup>48</sup> The expression also provides a quantification of mobility,

$$D_{ij}^\circ = \omega_{ij} k_B T \text{ and } \omega_{ij} = \frac{1}{6\pi\eta_j r_i}, \quad (9)$$

where  $\omega_{ij}$  is the mobility of molecule  $i$  in solvent  $j$ ,  $\eta_j$  is the dynamic viscosity of the solvent,  $r_i$  is the radius of the spherical particle  $i$ , and  $D_{ij}^\circ$  is the infinite dilution diffusion coefficient of the particle  $i$  in solvent  $j$ . Equation (9) is in line with the analysis of mobility of the individual components by Leahy-Dios and Firoozabadi.<sup>61</sup> It shows that  $\omega_{ij}$  decreases with the increase in viscosity and with the decrease in diffusion coefficient. Equation (9) is also a starting point for diffusion coefficient correlations. Mobility defined in Eq. (9) has the same dimension as mobility defined by de Groot and Mazur.<sup>6</sup>

According to Kramers and Broeder,<sup>69</sup> the Chapman theory describes the thermal diffusion in suspended particles from the change of constituents' mobility with temperature and to a less

extent to size and shape (an interpretation for similarity). Kramers and Broeder<sup>69</sup> also state that thermal diffusion in liquids is due to mobility dependency on temperature.

The similarity of components in a mixture is related to the response to the thermal driving force. Physical properties such as latent heat of vaporization may be related to similarity.<sup>61,62</sup> These properties are ultimately related to the molecular shape and size and to microscopic interactions. Blanco *et al.*<sup>29</sup> use the difference in molecular weight of the *n*-alkanes in a binary *n*-alkane mixture as a measure of similarity. A few authors<sup>70,71</sup> have used the solubility parameters to account for similarity. The main drawbacks are the dependence of the solubility parameters on the calculation method and that some simple mixtures (benzene-carbon tetrachloride and benzene-cyclohexane) do not follow the solubility parameter rule.<sup>62,70</sup> Leahy-Dios *et al.*<sup>62</sup> have used the difference in the net heat of transports ( $Q_1^* - Q_2^*$ ) in binary mixtures of *n*-alkanes and *n*-alkane-1-methylnaphthalene as a measure of similarity. The net heat of transport of component *i* ( $Q_i^*$ ) is defined according to

$$Q_i^* = Q_i - \bar{H}_i, \quad (10)$$

where  $Q_i$  is the heat of transport, defined as the amount of energy transported by diffusion flow per mole of component *i* across a reference plane when there is no temperature gradient,<sup>72,73</sup> and  $\bar{H}_i$  is the partial molar enthalpy of component *i*. The net heat of transport is then the amount of heat that must be absorbed by a given region to maintain temperature and pressure constant when 1 mol of component *i* flows out of that region.<sup>74</sup> According to the model of Dougherty and Drickamer,<sup>73</sup> the net heat of transport ( $Q_i^*$ ) can be understood as a combination of two energy terms: (a) the energy to detach a molecule from its surroundings and (b) the energy given up by the region when a molecule fills a hole. It is important to notice that  $Q_i^*$  is a function of the energy interactions of molecule *i* with its surroundings and includes the contributions of size and shape. Thus,  $Q_i^*$  of each component depends on the binary mixture and composition. The use of ( $Q_1^* - Q_2^*$ ) as a measure of similarity has the advantage that it accounts for the interaction energy of the molecules, influence of size and shape, the energy a molecule carries when it moves in a medium and the energy given up by the region when a molecule fills a space left by another molecule.

In this work, we use the interpretation of Leahy-Dios and Firoozabadi<sup>61</sup> and Leahy-Dios *et al.*<sup>62</sup> for mobility and similarity to analyze our thermodiffusion data. The mobility is accounted for qualitatively using the properties that influences it (i.e., mixture viscosity and pure component self-molecular diffusion coefficients and viscosities) and quantitatively by the Maxwell-Stefan diffusion coefficient ( $\mathcal{D}_{12}$ ). The similarity is evaluated from the difference in the net heat of transport ( $\Delta Q^* = Q_1^* - Q_2^*$ ).

The normalized molecular weight ( $MW_n$ , i.e., molecular weight of the *n*-alkane divided by the molecular weight of isobutylbenzene) is used to evaluate how mobility and similarity vary with the alkane chain length. Larger  $MW_n$  indicates a longer *n*-alkane in the isobutylbenzene-*n*-alkane mixtures. In binary mixtures containing *n*-alkanes, the dynamic viscosity of the mixture and Fickian diffusion coefficient decrease as  $MW_n$  increases at constant concentration.

The thermal diffusion factor  $\alpha_T$  (different from thermal diffusivity  $\alpha$ ) is defined by<sup>62,73–76</sup>

$$\alpha_T = T \frac{D_T}{D_{12}}. \quad (11)$$

The thermal diffusion factor can be described in terms of the net heats of transport ( $Q_1^* - Q_2^*$ ),<sup>73,76</sup>

$$\alpha_T = \frac{(Q_1^* - Q_2^*)}{x_1 \left( \frac{\partial \mu_1}{\partial x_1} \right)_{T,P}}, \quad (12)$$

where  $\mu_1$  and  $x_1$  are, respectively, the chemical potential and molar fraction of component 1.

One may express the chemical potential of component 1 in terms of its fugacity coefficient in the mixture ( $\hat{\phi}_1$ ). Then, using the relation between Fickian and Maxwell-Stefan diffusion coefficients ( $\mathcal{D}_{12}$ ) in a binary mixture,<sup>77</sup> Eqs. (11) and (12) are combined to obtain<sup>62</sup>

$$D_T = \frac{(Q_1^* - Q_2^*) \mathcal{D}_{12}}{RT^2 \left[ 1 + x_1 \left( \frac{\partial \ln \hat{\phi}_1}{\partial x_1} \right)_{P,T} \right]} = \frac{\Delta Q^* \mathcal{D}_{12}}{RT^2}. \quad (13)$$

We can calculate  $\mathcal{D}_{12}$  using the measured data of  $D_{12}$  divided by the thermodynamic factor  $\Gamma = 1 + x_1 \left( \frac{\partial \ln \hat{\phi}_1}{\partial x_1} \right)_{P,T}$ . The term  $1 + x_1 \left( \frac{\partial \ln \hat{\phi}_1}{\partial x_1} \right)_{P,T}$  is a measure of nonideality in mixtures<sup>77,78</sup> and can be calculated using an appropriate equation of state (EOS). In this work, we evaluate  $\Gamma$  from the Peng-Robinson equation of state (PR-EOS)<sup>79</sup> assuming the binary interaction parameter  $\delta_{ij}$  to be zero. After calculating  $\mathcal{D}_{12}$ ,  $\Delta Q^*$  is calculated by direct use of Eq. (13) and the measured  $D_T$ .

Equation (13) shows that  $D_T$  increases with the increase in  $\Delta Q^*$  as was first found out by Leahy-Dios *et al.*<sup>62</sup> If the chemical species 1 and 2 are the same, there will be no separation, and then both  $D_T$  and  $\Delta Q^*$  would be zero. The higher  $\Delta Q^*$ , the less similar are the components. We define  $\Delta Q^*$  as disparity and  $1/\Delta Q^*$  as similarity, as is defined in the literature.<sup>62</sup>

From measured  $D_{12}$  and  $D_T$ , Eq. (13) can be used to evaluate the contributions of concentration and hydrocarbon chain length in terms of mobility and similarity in Fickian diffusion and thermal diffusion coefficients.

### III. RESULTS AND DISCUSSION

#### A. Contrast factors

The concentration and temperature contrast factors for the toluene-*n*C<sub>6</sub> and IBB-*n*C<sub>12</sub> mixtures at 25 °C are presented in Table II which includes also literature data. Our  $(\partial n/\partial c_1)_{P,T}$  deviate from -0.17% to 1.66% when compared to literature data. The deviations are from (1) the uncertainties of the refractometer and balance in weighing the components (expected to be small) and (2) the difference in the wavelength of the refractometer and laser source (expected to be larger than the first), which may contribute to deviations of around 1.0%.<sup>4</sup>

Gebhardt *et al.*<sup>21</sup> report  $(\partial n/\partial c_1)_{P,T}$  at 25 °C for the IBB-*n*C<sub>12</sub> mixture at different concentrations for two different wavelengths



**TABLE II.** Contrast factors  $(\partial n/\partial c_1)_{P,T}$  and  $(\partial n/\partial T)_{P,c}$  of binary mixtures of toluene(tol)-*n*-alkane( $nC_i$ ) and isobutylbenzene(IBB)-*n*-alkane( $nC_i$ ) at different concentrations of toluene and isobutylbenzene ( $c_1$ ) at 25 °C and 1 atm.

Mixture	$c_1$ (mass fraction)	$(\partial n/\partial c_1)_{P,T}$ (mass fraction basis)		$(\partial n/\partial T)_{P,c}$ ( $10^{-4} \text{ K}^{-1}$ )	
		This work	Literature	This work	Literature
tol- $nC_6$	0.000	...	...	-5.412	-5.433 <sup>80</sup>
	0.262	0.1041	0.1024 <sup>80</sup>	-5.456	-5.457 <sup>80</sup>
	0.517	0.1200	0.1202 <sup>80</sup>	-5.504	-5.500 <sup>80</sup>
	0.762	0.1382	0.1372 <sup>80</sup>	-5.528	-5.564 <sup>80</sup>
	0.953	0.1510	0.1505 <sup>80</sup>	-5.620	-5.628 <sup>80</sup>
	1.000	...	...	-5.638	-5.648 <sup>80</sup>
IBB- $nC_{12}$	0.000	...	...	-4.304	-4.33 <sup>21</sup>
	0.100	0.0540	0.0536 <sup>21</sup>	-4.370	-4.36 <sup>21</sup>
	0.300	0.0585	0.0577 <sup>21</sup>	-4.412	-4.44 <sup>21</sup>
	0.500	0.0628	0.0625 <sup>21</sup>	-4.544	-4.56 <sup>21</sup>
	0.700	0.0687	0.0680 <sup>21</sup>	-4.670	-4.67 <sup>21</sup>
	0.900	0.0744	0.0741 <sup>21</sup>	-4.806	-4.82 <sup>21</sup>
	1.000	...	...	-4.892	-4.90 <sup>21</sup>

(405 and 633 nm). We use IBB as the reference component, which will change the sign reported by Gebhardt *et al.*<sup>21</sup> The average absolute deviation for our  $(\partial n/\partial c_1)_{P,T}$  and literature data for IBB- $nC_{12}$  (633 nm) is 0.81%. The data of Li *et al.*<sup>80</sup> are used to compare  $(\partial n/\partial c_1)_{P,T}$  at 25 °C and a wavelength of 633 nm for the tol- $nC_6$  mixture with our data, showing absolute average deviations of around 0.72%.

The pure component  $(\partial n/\partial T)_{P,c}$  can be used as a measure of the apparatus precision. Since for a pure component, there is no concentration gradient, we directly determine  $(\partial n/\partial T)_{P,c}$  from solution of Eqs. (2)–(4) based on the steady state deflection of the laser beam. The absolute deviation of  $(\partial n/\partial T)_{P,c}$  in comparison to the literature<sup>21,80</sup> ranges from 0.16% to 0.39% for the pure components (toluene, IBB,  $nC_6$ , and  $nC_{12}$ ), which is an indication of a small  $\Delta T$  measurement error.

Our values of  $(\partial n/\partial T)_{P,c}$  for the system IBB- $nC_{12}$  have a maximum absolute deviation of 0.63% with literature data. Königer *et al.*<sup>41</sup> report a value of  $(-4.54 \pm 0.02) \times 10^{-4} \text{ K}^{-1}$  for the mixture of IBB- $nC_{12}$  at a mass fraction of 0.50. The dispersion in data of Königer *et al.*<sup>41</sup> ( $\pm 0.02 \times 10^{-4}$ ) is around  $\pm 0.44\%$  which is close to the deviations with ours. Our  $(\partial n/\partial T)_{P,c}$  for the tol- $nC_6$  mixture has a maximum deviation of -0.65% from data of Li *et al.*<sup>80</sup> at  $c_1 = 0.762$ .

The contrast factors for the binary mixtures of IBB and *n*-alkanes ( $nC_6$ ,  $nC_8$  and  $nC_{10}$ ) are provided in Table III. The dispersion of our estimated  $(\partial n/\partial T)_{P,c}$  ranges from  $\pm 10^{-6}$  to  $\pm 4 \times 10^{-6}$ . The temperature contrast factors should have very high accuracy. An error of 5% ( $\sim 2.5 \times 10^{-5}$ ) in  $(\partial n/\partial T)_{P,c}$  may lead to a large error (as large as 100% or more in some composition range) in  $D_T$  and  $S_T$  as we demonstrate in the Appendix.

## B. Validation and diffusion coefficients

First, we validate our measurements at the entire concentration range for the mixtures of toluene-*n*-hexane (tol- $nC_6$ ) and

isobutylbenzene-*n*-dodecane (IBB- $nC_{12}$ ). Our measured data for  $D_{12}$ ,  $D_T$ , and  $S_T$  for the tol- $nC_6$  mixtures are compared to the literature data in Table IV and in Fig. 3.

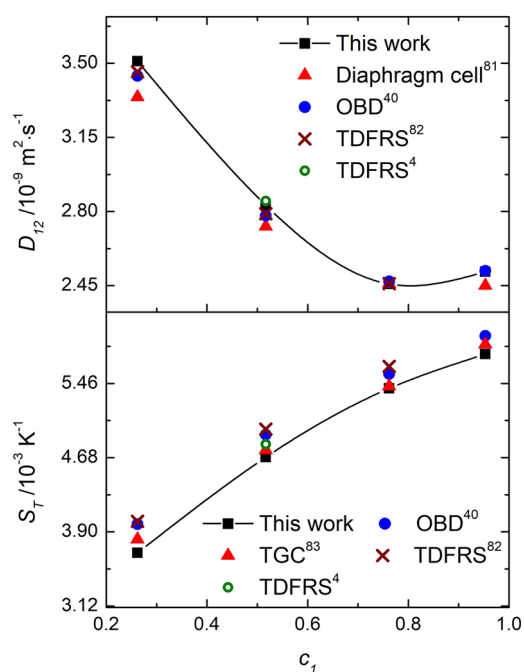
The absolute deviations of  $D_{12}$ ,  $S_T$ , and  $D_T$  for the tol- $nC_6$  mixtures from our measurements and literature data range from close to 0%–3.85% for  $D_{12}$ , 0.37%–8.23% for  $S_T$  and 1.16%–7.35% for  $D_T$ . The dispersion of the data from the literature is comparable to the deviations from our work. A higher absolute deviation of 8.2% in  $S_T$

**TABLE III.** Contrast factors  $(\partial n/\partial c_1)_{P,T}$  and  $(\partial n/\partial T)_{P,c}$  of binary mixtures of isobutylbenzene (IBB) and *n*-alkanes ( $nC_i$ ) at different concentrations ( $c_1$ ) of isobutylbenzene at 25 °C and 1 atm.

System	$c_1$ (mass fraction)	$(\partial n/\partial c_1)_{P,T}$ (mass fraction basis)	$(\partial n/\partial T)_{P,c}$ ( $10^{-4} \text{ K}^{-1}$ )
IBB- $nC_6$	0.100	0.0916	-5.382
	0.300	0.1012	-5.257
	0.500	0.1112	-5.137
	0.700	0.1213	-5.036
	0.900	0.1317	-4.925
IBB- $nC_8$	0.100	0.0744	-4.807
	0.300	0.0805	-4.819
	0.500	0.0876	-4.820
	0.700	0.0957	-4.849
IBB- $nC_{10}$	0.900	0.1048	-4.885
	0.100	0.0617	-4.543
	0.300	0.0672	-4.600
	0.500	0.0733	-4.657
	0.700	0.0800	-4.722
	0.900	0.0873	-4.829

**TABLE IV.** Fickian diffusion ( $D_{12}$ ), thermal diffusion ( $D_T$ ), and Soret ( $S_T$ ) coefficients of binary mixtures of toluene and  $n$ -hexane at different concentrations of toluene ( $c_1$ ) at 25 °C and 1 atm from the literature<sup>4,40,81–83</sup> and this work.

$c_1$ (mass fraction)	$D_{12}$ ( $10^{-9}$ m <sup>2</sup> s <sup>-1</sup> )		$S_T$ ( $10^{-3}$ K <sup>-1</sup> )		$D_T$ ( $10^{-12}$ m <sup>2</sup> s <sup>-1</sup> K <sup>-1</sup> )	
	This work	Literature	This work	Literature	This work	Literature
0.262	3.51 ± 0.12	3.44 <sup>a,40</sup> 3.37 <sup>c,81</sup> 3.46 <sup>d,82</sup>	3.68 ± 0.04	3.98 <sup>a,40</sup> 4.01 <sup>d,82</sup> 3.82 <sup>b,83</sup>	12.91 ± 0.45	12.77 <sup>b,4</sup> 13.69 <sup>a,e,40</sup> 13.87 <sup>d,e,82</sup>
0.517	2.83 ± 0.01	2.85 <sup>d,4</sup> 2.78 <sup>a,40</sup> 2.76 <sup>c,81</sup> 2.79 <sup>d,82</sup>	4.68 ± 0.04	4.82 <sup>d,e,4</sup> 4.92 <sup>a,40</sup> 4.98 <sup>d,82</sup> 4.76 <sup>b,83</sup>	13.25 ± 0.11	13.73 <sup>d,4</sup> 13.70 <sup>b,4</sup> 13.68 <sup>a,e,40</sup> 13.89 <sup>d,e,82</sup>
0.762	2.46 ± 0.04	2.47 <sup>a,40</sup> 2.46 <sup>c,81</sup> 2.49 <sup>d,82</sup>	5.41 ± 0.02	5.56 <sup>a,40</sup> 5.64 <sup>d,82</sup> 5.43 <sup>b,83</sup>	14.29 ± 0.19	13.73 <sup>a,e,40</sup> 14.04 <sup>d,e,82</sup>
0.953	2.52 ± 0.09	2.52 <sup>a,40</sup> 2.45 <sup>c,81</sup>	5.77 ± 0.34	5.96 <sup>a,40</sup> 5.87 <sup>b,83</sup>	14.52 ± 1.15	15.02 <sup>a,e,40</sup>

<sup>a</sup>OBD—optical beam deflection.<sup>b</sup>TGC—thermal gravitational column.<sup>c</sup>DC—Diaphragm cell. The data reported in Ref. 82 are measured at 23 °C.<sup>d</sup>TDFRS—thermal diffusion forced Rayleigh scattering.<sup>e</sup>Calculated from Eq. (6) using reported data in the reference.**FIG. 3.** Fickian diffusion ( $D_{12}$ ) and Soret ( $S_T$ ) coefficients of binary mixtures of toluene(1) and  $n$ -hexane(2) as a function of toluene concentration in mass fraction ( $c_1$ ) at 25 °C and 1 atm. Lines are tendency splines. TGC—thermal gravitational column, OBD—optical beam deflection, and TDFRS—thermal diffusion forced Rayleigh Scattering.

in the toluene mass fraction of 0.262 is observed from our measurement and data of Köhler and Müller.<sup>82</sup> Our measured  $S_T$  is in better agreement with Bou-Ali *et al.*,<sup>83</sup> with deviations ranging from 0.37% to 3.66%.

Our measurements for the IBB- $nC_{12}$  mixture are compared to literature data in Table V. The overall absolute deviations of  $D_{12}$ ,  $S_T$ , and  $D_T$  are, respectively, 4.1%, 5.5%, and 3.8%. The higher deviation is for the 0.10 IBB mass fraction. At 0.50 mass fraction, the deviation for  $D_T$  is 4.1%, within the dispersion reported for the benchmark mixture. The comparison shown in Fig. 4 has more spread in  $D_{12}$  from various measurements.

In the numerical solution, we fully reproduce the measured beam deflection, including the observed overshoot and the laser position fluctuations from the temperature variation, as shown in Fig. 5. There is a deviation in the peak of the overshoot of  $\sim 25$   $\mu\text{m}$ , corresponding to 0.55% deviation of the total deflection, which is very small.

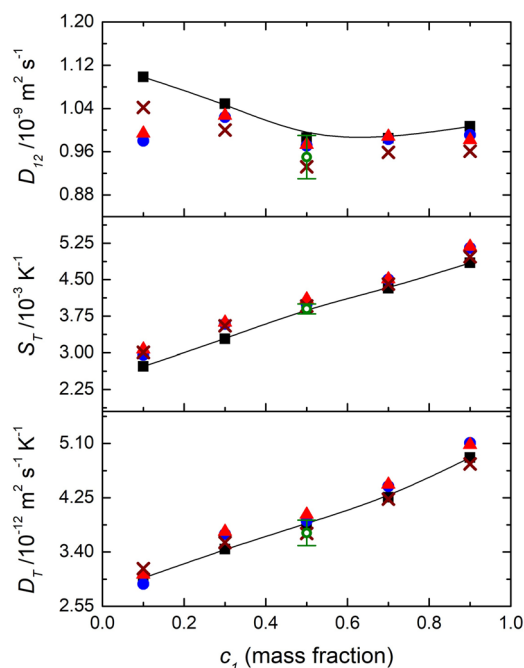
Our measurements ( $D_{12}$ ,  $D_T$ , and  $S_T$ ) for the 3 new binary mixtures (IBB- $nC_6$ , IBB- $nC_8$ , IBB- $nC_{10}$ ) in the entire concentration range are shown in Table VI. Our  $S_T$  and  $D_T$  data (IBB as the reference component) have a positive sign. A positive  $D_T$  for a given component in a binary mixture indicates it segregates in the cold side and thus it is thermophobic.

Hartmann *et al.*<sup>39</sup> report  $S_T = 6.81 \times 10^{-3} \text{ K}^{-1}$  for the equimolar binary mixture of IBB- $nC_6$  (mass fraction  $c_1 = 0.609$ ). The deviation between Hartmann *et al.*<sup>39</sup> and our interpolated  $S_T = 6.30 \times 10^{-3} \text{ K}^{-1}$  for a mass fraction of 0.609 (equimolar mixture) is 7.5%.

Blanco *et al.*<sup>84</sup> report  $D_T$  for the IBB- $nC_{10}$  mixture at 0.50 mass fraction to be  $6.01 \times 10^{-12} \text{ m}^2 \text{ s}^{-1} \text{ K}^{-1}$ . Rahman<sup>85</sup> reports  $D_{12}$

**TABLE V.** Fickian diffusion ( $D_{12}$ ), thermal diffusion ( $D_T$ ), and Soret ( $S_T$ ) coefficients of binary mixtures of isobutylbenzene (IBB) and  $n$ -dodecane ( $nC_{12}$ ) at different concentrations of isobutylbenzene at 25 °C and 1 atm from the literature<sup>15,21</sup> and this work.

$c_1$ (mass fraction)	$D_{12}$ ( $10^{-9} \text{ m}^2 \text{ s}^{-1}$ )		$S_T$ ( $10^{-3} \text{ K}^{-1}$ )		$D_T$ ( $10^{-12} \text{ m}^2 \text{ s}^{-1} \text{ K}^{-1}$ )	
	This work	Literature <sup>15,21</sup>	This work	Literature <sup>15,21</sup>	This work	Literature <sup>15,21</sup>
0.100	$1.10 \pm 0.06$	0.980	$2.72 \pm 0.07$	2.96	$2.99 \pm 0.18$	2.90
		0.994		3.07		3.05
		1.042		3.01		3.14
0.300	$1.05 \pm 0.04$	1.024	$3.28 \pm 0.05$	3.59	$3.44 \pm 0.14$	3.68
		1.027		3.62		3.72
		1.000		3.55		3.55
0.500	$0.99 \pm 0.02$	0.971	$3.90 \pm 0.05$	4.00	$3.86 \pm 0.04$	3.89
		0.973		4.10		3.99
		0.932		3.96		3.69
		$0.95 \pm 0.04$ (benchmark)		$3.9 \pm 0.1$ (benchmark)		$3.7 \pm 0.2$ (benchmark)
0.700	$0.98 \pm 0.01$	0.983	$4.32 \pm 0.06$	4.50	$4.23 \pm 0.07$	4.43
		0.988		4.51		4.46
		0.959		4.41		4.23
0.900	$1.01 \pm 0.03$	0.991	$4.85 \pm 0.09$	5.15	$4.90 \pm 0.14$	5.11
		0.982		5.18		5.08
		0.961		4.97		4.78

**FIG. 4.** Fickian diffusion ( $D_{12}$ ), Soret ( $S_T$ ), and thermal diffusion ( $D_T$ ) coefficients vs isobutylbenzene concentration in mass fraction ( $c_1$ ). Isobutylbenzene(1)- $n$ -dodecane(2) at 25 °C and 1 atm. Black squares: this work; blue circles: optical beam deflection (405 nm);<sup>21</sup> red triangles: optical beam deflection (633 nm);<sup>21</sup> brown crosses: optical beam deflection (670 nm);<sup>21</sup> and empty green circles: Fontainebleau benchmark.<sup>15</sup> Lines are tendency splines.

( $0.52 \times 10^{-9} \text{ m}^2 \text{ s}^{-1}$ ) and  $S_T$  ( $4.13 \times 10^{-3} \text{ K}^{-1}$ ) for the same mixture and concentration. Using Rahman's<sup>85</sup> data and Eq. (6), one can calculate  $D_T$  for the IBB- $nC_{10}$  mixture to be  $2.15 \times 10^{-12} \text{ m}^2 \text{ s}^{-1} \text{ K}^{-1}$ . Our value for  $D_T$  ( $5.47 \times 10^{-12} \text{ m}^2 \text{ s}^{-1} \text{ K}^{-1}$ ) is close to the value of Blanco *et al.*;<sup>84</sup> the difference is around 9%.

### C. Effect of molecular size of $n$ -alkane on the Fickian and thermal diffusion coefficients

Figure 6 shows that  $D_{12}$  decreases with the increase in the normalized molecular weight  $MW_n$  (molecular weight of  $n$ -alkane divided by molecular weight of isobutylbenzene) in the IBB- $n$ -alkane mixtures. A power law fit describes all the data points, like other aromatic- $n$ -alkane mixtures such as 1-methylnaphthalene- $n$ -alkane systems.<sup>61</sup> Our measurements of  $D_{12}$  may be analyzed in terms of the  $n$ -alkane mobility, which is a function of self-molecular diffusion coefficient ( $D_i$ ) and dynamic viscosity ( $\eta_i$ ).  $D_i$  and  $\eta_i$  for the  $n$ -alkanes in this work follow ( $D_{nC_6} > D_{nC_8} > D_{nC_{10}} > D_{nC_{12}}$ )<sup>65</sup> and ( $\eta_{nC_6} < \eta_{nC_8} < \eta_{nC_{10}} < \eta_{nC_{12}}$ ),<sup>49</sup> indicating that the solvent mobility decreases as the  $n$ -alkane chain length increases. This observation leads to the conclusion that a decrease in solvent mobility should lead to a decrease in  $D_{12}$  for a fixed concentration. This is what we observe in our data.

We examine the similarity effect in  $D_{12}$  using the same reasoning as Leahy-Dios and Firoozabadi,<sup>61</sup> comparing Fickian diffusion coefficients of different aromatic- $n$ -alkane and  $n$ -alkane- $n$ -alkane mixtures at the same concentration. Figure 7 depicts literature data and our measured Fickian diffusion coefficient as a function of molecular weight of  $n$ -alkanes in equimass mixtures of toluene (tol), 1-methylnaphthalene (MN), isobutylbenzene (IBB), and  $n$ -decane

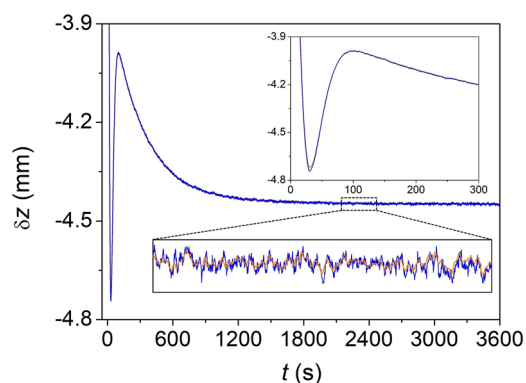


**FIG. 5.** Variation of the measured laser deflection  $\delta z$  (blue) vs time ( $t$ ) and predictions (orange) from the estimated parameters ( $D_{12}$ ,  $D_T$ , and  $(\partial n/\partial T)_{P,c}$ ) for the IBB- $nC_{12}$  mixture at 50% mass fraction. Fluctuation at steady state:  $\pm 3$  to  $5 \mu\text{m}$ . The parameters determined for this specific run are  $D_{12} = 1.00 \times 10^{-9} \text{ m}^2 \text{ s}^{-1}$ ,  $D_T = 3.87 \times 10^{-12} \text{ m}^2 \text{ s}^{-1} \text{ K}^{-1}$ , and  $(\partial n/\partial T)_{P,c} = -4.525 \times 10^{-4} \text{ K}^{-1}$ .

( $nC_{10}$ ). The self-diffusion coefficient ( $D_i$ ) and dynamic viscosity ( $\eta_i$ ) of these pure solvents at  $25^\circ\text{C}$  and 1 atm vary according to  $D_{\text{tol}}^{87} > D_{nC_{10}}^{65} > D_{\text{IBB}} > D_{\text{MN}}$  and  $\eta_{\text{tol}} < \eta_{nC_{10}} < \eta_{\text{IBB}} < \eta_{\text{MN}}$ ,<sup>49,88–90</sup> indicating that mobility is the highest for toluene and the lowest for 1-methylnaphthalene in the group of components. We have estimated the self-diffusion coefficients of IBB and MN using the Stokes-Einstein equation [Eq. (9)]. The dynamic viscosity of IBB at  $25^\circ\text{C}$  and 1 atm is estimated by extrapolating the literature data.<sup>88–90</sup>

Based on mobility alone, the Fickian diffusion coefficients of the mixtures shown in Fig. 7 should follow  $D_{nC_i\text{-tol}}^{36} > D_{nC_i\text{-}nC_{10}}^{61,86} > D_{nC_i\text{-IBB}} > D_{nC_i\text{-MN}}^{36}$ . Indeed, this is the case. The results suggest that Fickian diffusion coefficient of a given mixture is dominated by the solvent mobility, in line with the literature.<sup>61</sup>

Figure 8 shows  $D_T$  (isobutylbenzene as reference compound) as a function of the normalized molecular weight ( $MW_n$ ) for the entire range of concentration.

The  $D_T$  vs  $MW_n$  for the IBB- $nC_i$  mixtures can be described by a power law fit. The same behavior has been observed in equimass binary mixtures of MN- $nC_i$ ,<sup>36,61</sup> tol- $nC_i$ ,<sup>36</sup> and benzene- $nC_i$ ,<sup>91</sup> suggesting a general trend for the aromatic- $n$ -alkane mixtures. Thermal diffusion  $D_T$  data for the  $n$ -alkane- $n$ -alkane mixtures are described by a second order polynomial fit as reported by Larrañaga *et al.*<sup>36</sup> (based on the data of Blanco *et al.*<sup>29</sup> and Leahy-Dios and Firoozabadi<sup>61</sup>).

According to Fig. 9, the mobility ( $D_{12}$ ) and disparity ( $\Delta Q^*$ ) decrease as  $MW_n$  increases. The result is a decrease in  $D_T$  with increase in  $MW_n$ . Decrease in  $D_T$  with increase in  $MW_n$  for aromatic- $n$ -alkane mixtures at fixed concentration has been observed by various authors.<sup>5,36,61,62,91</sup> The results suggest that the general contribution of similarity ( $1/\Delta Q^*$ ) observed by other authors<sup>62</sup> for the mixtures of 1-methylnaphthalene- $n$ -alkane (i.e., similarity increases with the normalized molecular weight leading  $D_T$  to decrease) is also valid for the IBB- $nC_i$  mixtures.

The decrease in mobility with the increase in  $MW_n$  (Fig. 9) may be related to the increase in the mixture dynamic viscosity, and the decrease in self-diffusion coefficient of the  $n$ -alkane solvents as the number of  $n$ -alkane carbon atoms increases.

**TABLE VI.** Fickian diffusion ( $D_{12}$ ), thermal diffusion ( $D_T$ ), and Soret ( $S_T$ ) coefficients of binary mixtures of isobutylbenzene (IBB) and  $n$ -alkanes ( $nC_i$ ) at different concentrations of isobutylbenzene at  $25^\circ\text{C}$  and 1 atm.

Mixture	$c_1$ (mass fraction)	$D_{12}$ ( $10^{-9} \text{ m}^2 \text{ s}^{-1}$ )	$S_T$ ( $10^{-3} \text{ K}^{-1}$ )	$D_T$ ( $10^{-12} \text{ m}^2 \text{ s}^{-1} \text{ K}^{-1}$ )
IBB- $nC_6$	0.100	$3.09 \pm 0.08$	$5.12 \pm 0.09$	$15.82 \pm 0.16$
	0.300	$2.57 \pm 0.02$	$5.77 \pm 0.03$	$14.83 \pm 0.07$
	0.500	$2.21 \pm 0.02$	$6.17 \pm 0.04$	$13.64 \pm 0.17$
	0.700	$1.93 \pm 0.01$	$6.34 \pm 0.03$	$12.24 \pm 0.08$
	0.900	$1.74 \pm 0.01$	$6.23 \pm 0.05$	$10.84 \pm 0.11$
IBB- $nC_8$	0.100	$2.16 \pm 0.05$	$3.98 \pm 0.22$	$8.60 \pm 0.58$
	0.300	$1.77 \pm 0.02$	$4.69 \pm 0.04$	$8.30 \pm 0.10$
	0.500	$1.59 \pm 0.01$	$5.18 \pm 0.03$	$8.24 \pm 0.09$
	0.700	$1.47 \pm 0.01$	$5.54 \pm 0.02$	$8.14 \pm 0.05$
	0.900	$1.38 \pm 0.04$	$5.53 \pm 0.06$	$7.63 \pm 0.17$
IBB- $nC_{10}$	0.100	$1.42 \pm 0.04$	$3.39 \pm 0.05$	$4.81 \pm 0.11$
	0.300	$1.30 \pm 0.04$	$3.99 \pm 0.05$	$5.19 \pm 0.13$
	0.500	$1.21 \pm 0.01^a$	$4.52 \pm 0.03^a$	$5.47 \pm 0.07^{a,b}$
	0.700	$1.15 \pm 0.01$	$4.98 \pm 0.02$	$5.73 \pm 0.03$
	0.900	$1.15 \pm 0.01$	$5.22 \pm 0.02$	$6.00 \pm 0.05$

<sup>a</sup>Reference 85 reports  $D_{12} = 0.52 \times 10^{-9} \text{ m}^2 \text{ s}^{-1}$  and  $S_T = 4.13 \times 10^{-3} \text{ K}^{-1}$ , use of Eq. (6) results in  $D_T = 2.15 \times 10^{-12} \text{ m}^2 \text{ s}^{-1} \text{ K}^{-1}$ .

<sup>b</sup>Reference 84 reports  $D_T = 6.01 \times 10^{-12} \text{ m}^2 \text{ s}^{-1} \text{ K}^{-1}$ .

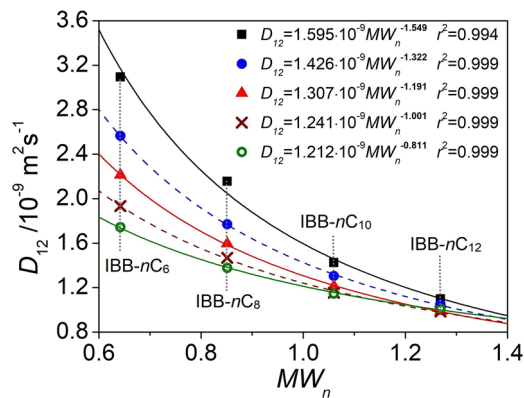


**FIG. 6.** Fickian diffusion coefficients ( $D_{12}$ ) vs normalized molecular weight  $MW_n$  (molecular weight of  $n$ -alkane divided by molecular weight of isobutylbenzene) for the isobutylbenzene(IBM)- $n$ -alkane( $nC_i$ ) ( $i = 6, 8, 10,$  and  $12$ ) binary mixtures. Symbols are used to define the concentration in mass fraction of IBM ( $c_1$ ): black squares are 0.10, blue circles are 0.30, red triangles are 0.50, brown crosses are 0.70, and empty green circles are 0.90 (dashed and solid lines are power law adjustments).

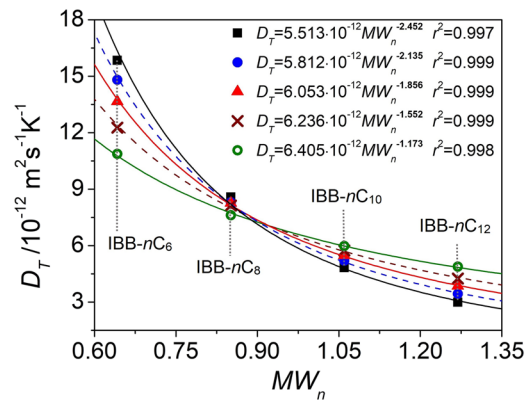


**FIG. 8.** Thermal diffusion coefficients ( $D_T$ ) vs normalized molecular weight  $MW_n$  (molecular weight of  $n$ -alkane divided by molecular weight of isobutylbenzene) for the isobutylbenzene(IBM)- $n$ -alkane( $nC_i$ ) ( $i = 6, 8, 10, 12$ ) binary mixtures. Symbols define the mass fraction of IBM ( $c_1$ ): black squares, 0.10; blue circles, 0.30; red triangles, 0.50; brown crosses, 0.70; and empty green circles, 0.90. Dashed and solid lines are power law fits.

A crossover point is observed at  $MW_n$  around 0.9 in Fig. 8. This trend will be discussed next as part of the concentration dependency of  $D_T$ .

#### D. Concentration dependence of Fickian diffusion and thermal diffusion coefficients

Figure 10 shows dependency of  $D_{12}$  and  $D_T$  on concentration in the binary mixtures. The Fickian diffusion coefficient dependence on concentration is better correlated by a second order polynomial. This observed behavior is different for the  $n$ -alkane- $n$ -alkane mixtures,<sup>86</sup> which show linear variation. An increase in IBM concentration generally decreases  $D_{12}$ . This behavior in the IBM- $nC_6$  and

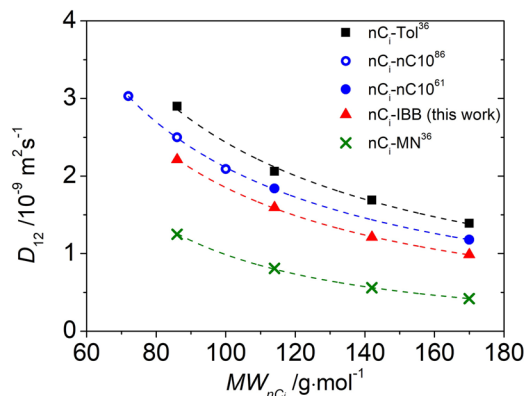


**FIG. 7.** Fickian diffusion coefficients ( $D_{12}$ ) vs molecular weight of the  $n$ -alkane solvent ( $MW_{nCi}$ ) for different equimass binary mixtures. Dashed lines are power law adjustments.

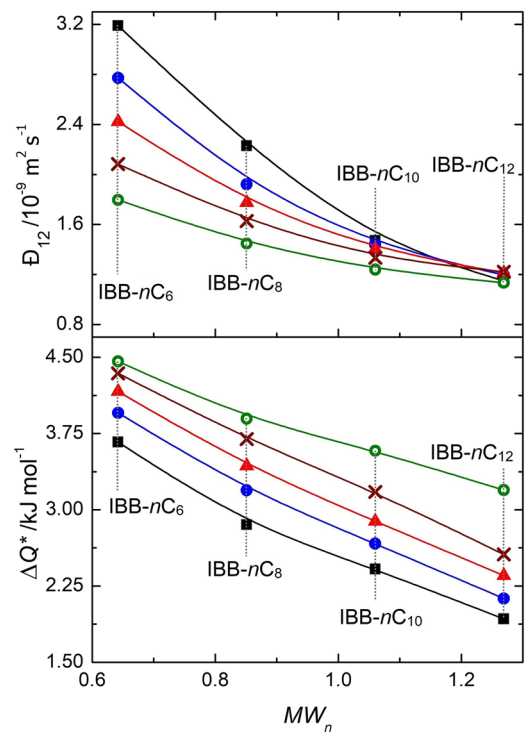


**FIG. 9.** Mobility ( $D_{12}$ ) and disparity ( $\Delta Q^*$ ) vs normalized molecular weight  $MW_n$  (molecular weight of  $n$ -alkane divided by molecular weight of isobutylbenzene) for the isobutylbenzene(IBM)- $n$ -alkane( $nC_i$ ) ( $i = 6, 8, 10, 12$ ) binary mixtures. Symbols define the mass fraction of IBM; black squares, 0.10; blue circles, 0.30; red triangles, 0.50; brown crosses, 0.70; and empty green circles, 0.90. Solid lines are splines fits to the data.

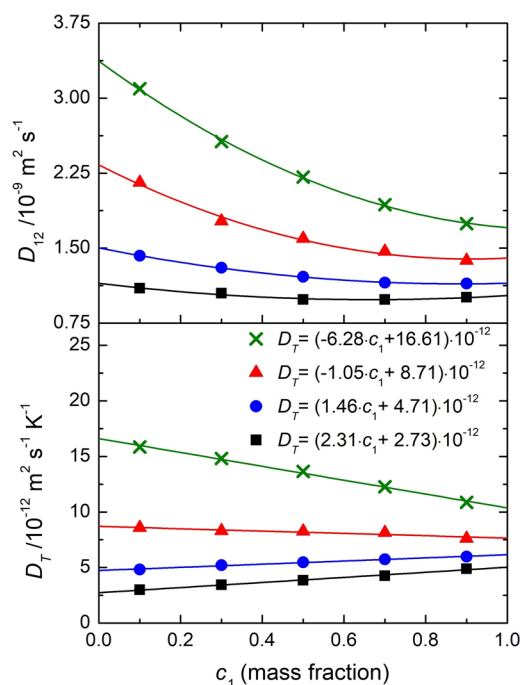


**FIG. 10.** Fickian diffusion ( $D_{12}$ ) and thermal diffusion ( $D_T$ ) coefficients vs isobutylbenzene concentration in mass fraction for different isobutylbenzene (IBB)- $n$ -alkanes ( $nC_i$ ) ( $i = 6, 8, 10, 12$ ) binary mixtures at 25 °C and 1 atm. Black squares: IBB- $nC_{12}$ ; blue circles: IBB- $nC_{10}$ ; red triangles: IBB- $nC_8$ ; and green crosses: IBB- $nC_6$ .  $D_{12}$  solid lines: quadratic polynomial fit;  $D_T$  solid lines: linear fittings.

IBB- $nC_8$  mixtures can be partly related to the increase in mixture viscosity with the increase in IBB concentration; IBB has a higher dynamic viscosity than  $n$ -hexane and  $n$ -octane. We observe that  $D_{12}$  dependence on concentration becomes weaker as the number of carbon atoms in  $n$ -alkane increases. We have analyzed the results of Polyakov *et al.*<sup>34</sup> for the mixtures of benzene- $nC_7$  and benzene- $nC_{13}$  (data extracted from the graph and molar fraction converted to mass fraction) and observe the same behavior. The data of Polyakov *et al.*<sup>34</sup>  $D_{12}$  have a weak or no dependence on benzene concentration for the benzene- $nC_{13}$  mixture and show a nonlinear variation to mass fraction for the benzene- $nC_7$  mixture.

**TABLE VII.** Fickian diffusion ( $D_{ij}^\circ$ ) and thermal diffusion ( $D_{Tj}^\circ$ ) coefficients at infinite dilution in binary mixtures of isobutylbenzene (IBB—component 1) and  $n$ -alkanes ( $nC_i$ —component 2) at 25 °C and 1 atm.

Mixture	$D_{12}^\circ$ ( $10^{-9} \text{ m}^2 \text{ s}^{-1}$ )	$D_{21}^\circ$ ( $10^{-9} \text{ m}^2 \text{ s}^{-1}$ )	$D_{T1}^\circ$ ( $10^{-12} \text{ m}^2 \text{ s}^{-1} \text{ K}^{-1}$ )	$D_{T2}^\circ$ ( $10^{-12} \text{ m}^2 \text{ s}^{-1} \text{ K}^{-1}$ )
IBB- $nC_6$	3.371	1.705	16.61	10.34
IBB- $nC_8$	2.332	1.401	8.71	7.66
IBB- $nC_{10}$	1.500	1.149	4.71	6.17
IBB- $nC_{12}$	1.148	1.025	2.73	5.04

The Fickian diffusion coefficients of component  $i$  infinitely diluted in component  $j$  ( $D_{ij}^\circ$ ) are listed in Table VII. The infinite dilution diffusion coefficients are obtained by extrapolation of the quadratic dependence of  $D_{12}$  with mass fraction to the dilution extrema.

De Mezquia *et al.*<sup>86</sup> show that in the  $n$ -alkane- $n$ -alkane mixtures at a mass fraction of 0.5, the product of the Fickian diffusion coefficient and mixture viscosity is constant ( $D_{12} \times \eta_{12} = k$ ). The same is also shown by Larrañaga *et al.*<sup>36</sup> for mixtures of tol- $nC_i$  and MN- $nC_i$ . We have estimated  $\eta_{12}$  using the Grunberg and Nissan method<sup>92</sup> with an interaction parameter calculated by the group contribution method proposed by Isdale *et al.*<sup>93</sup> as detailed in the work of Poling *et al.*<sup>48</sup> We find  $k = 1.12 \times 10^{-12} \text{ kg m s}^{-2}$  with a standard deviation of  $0.08 \times 10^{-12} \text{ kg m s}^{-2}$ . This deviation may be due to the error in the estimation of viscosity. Larrañaga *et al.*<sup>36</sup> observe that  $k$  depends on the aromatic molecule in an aromatic- $n$ -alkane mixture. They have found  $k = 1.09 \times 10^{-12} \text{ kg m s}^{-2}$  in the tol- $nC_i$  mixtures and  $0.7 \times 10^{-12} \text{ kg m s}^{-2}$  in the MN- $nC_i$  mixtures. For the  $n$ -alkane- $n$ -alkane mixtures,  $k$  is a constant<sup>86</sup> being equal to  $1.18 \times 10^{-12} \text{ kg m s}^{-2}$ .

Figure 10 shows the concentration dependency (IBB as component 1) of  $D_T$  in the IBB- $nC_i$  mixtures, which can be described by a straight line,

$$D_T = (D_{T2}^\circ - D_{T1}^\circ)c_1 + D_{T1}^\circ. \quad (14)$$

$D_{T1}^\circ$  ( $c_1 \rightarrow 0$ ) and  $D_{T2}^\circ$  ( $c_1 \rightarrow 1$ ) are the thermal diffusion coefficients at the infinite dilution of components 1 (IBB) and 2 ( $n$ -alkanes); see Table VII.

Other authors also point to the linearity between  $D_T$  and mass fraction in binary mixtures of aromatic- $n$ -alkane<sup>36</sup> (MN- $n$ -alkane and tol- $n$ -alkane) and  $n$ -alkane- $n$ -alkane.<sup>30,31</sup> The data from Polyakov *et al.*<sup>34</sup> for benzene- $nC_7$  and benzene- $nC_{13}$  follow the same trend.

The coefficient of determination  $r^2$  for the linear relationship in Eq. (14) (see Fig. 10) is higher than 0.99 for the IBB- $nC_6$ , IBB- $nC_{10}$  and IBB- $nC_{12}$  mixtures, while it is about 0.89 for the IBB- $nC_8$  mixture. The IBB- $nC_8$  mixture at  $MW_n = 0.85$  is close to the crossover point (Fig. 8;  $MW_n \approx 0.9$ ), where  $D_T$  does not show concentration dependency. The variation of  $D_T$  for the IBB- $nC_8$  mixture is about 12% over the whole range of concentration in Fig. 10.

Figure 8 shows the  $D_T$  dependency on concentration as a function of  $MW_n$ . When  $MW_n$  is greater than the crossover point

of 0.9,  $D_T$  increases with increase in IBB concentration, having a positive slope in the linear dependence on concentration. When  $MW_n$  is less than 0.9 (the crossover point),  $D_T$  decreases with IBB concentration increase, having a negative slope. The slope of  $D_T$  in Fig. 10 is intimately related to the crossover point in Fig. 8, approaching zero at  $MW_n \approx 0.9$  ( $D_{T2}^\circ - D_{T1}^\circ = 0$ ), indicating there is no concentration dependency at the crossover point. Accordingly, the thermal diffusion coefficient  $D_T$  of the IBB- $nC_9$  mixture ( $MW_n = 0.96$ ) at 25 °C is expected to vary from  $6.09 \times 10^{-12}$  to  $6.72 \times 10^{-12} \text{ m}^2 \text{ s}^{-1} \text{ K}^{-1}$  in the concentration range of 0.10–0.90 in IBB mass fraction.

Larrañaga *et al.*<sup>36</sup> have noted the slope change of  $D_T$  vs  $c_1$  plots for the MN- $nC_i$  mixtures. Their data shows the slope is nearly zero when  $MW_n$  corresponds to  $n$ -tetradecane (a crossover point). The data of Leahy-Dios *et al.* for the same mixtures (MN- $nC_i$ ) shows the crossover point at a different  $MW_n$ . The sign of the slope in the linear dependence of  $D_T$  with MN concentration changes from negative for MN- $nC_{14}$  to positive for MN- $nC_{16}$ . The thermodiffusion coefficients measured by Leahy-Dios *et al.*<sup>62</sup> for MN- $nC_{16}$  at mass fractions of 0.25 and 0.75 were, respectively,  $(4.10 \pm 0.08) \times 10^{-12} \text{ m}^2 \text{ s}^{-1} \text{ K}^{-1}$  and  $(4.18 \pm 0.06) \times 10^{-12} \text{ m}^2 \text{ s}^{-1} \text{ K}^{-1}$ . If the error in their data is considered, both values are the same, which means the crossover point is at a  $MW_n$  equivalent to MN- $nC_{16}$ . The sign of the slope does not change in the tol- $nC_i$  mixtures from Larrañaga *et al.*<sup>36</sup> In the tol- $nC_i$  mixtures,  $D_T$  increases with toluene concentration increase. The concentration dependency of  $D_T$  in the tol- $nC_i$  mixture weakens as the  $n$ -alkane molecular weight (i.e.,  $MW_n$ ) decreases. It seems that the increase in molecular weight of the aromatic in the mixtures of tol- $nC_i$ , IBB- $nC_i$ , and MN- $nC_i$  shifts the crossover point to higher  $MW_n$ . The existence and location of a crossover point in an aromatic- $n$ -alkane mixture may be a function of the functional groups and structure of the aromatic molecule and not only of the molecular weight of the mixture constituents. To shed light on the interpretation of the crossover point, we use the concepts of mobility and similarity.

The crossover may be analyzed by examining the dependency of mobility  $\mathcal{D}_{12}$  and disparity  $\Delta Q^*$  on concentration, as shown in Fig. 11. According to Eq. (13), thermal diffusion coefficients are given by the product of disparity ( $\Delta Q^*$ ) and mobility ( $\mathcal{D}_{12}$ ) divided by  $(RT^2)$ . Figure 11 shows that while disparity increases with IBB concentration increase in the IBB- $nC_i$  mixtures, mobility dependency on concentration weakens as  $MW_n$  increases (see Figs. 9 and 11). In this way, the change of the slope of the linear dependency of  $D_T$  with mass fraction (Fig. 10) is due to different types of variations of  $\Delta Q^*$  and  $\mathcal{D}_{12}$  with the IBB mass fraction (Fig. 11). The product ( $\Delta Q^* \times \mathcal{D}_{12}$ ) gives distinct variations in thermal diffusion coefficients with  $c_1$  in the IBB- $n$ -alkane mixtures. Consequently, the crossover in Fig. 8 and the slope change in Fig. 10 are the result of the combined effect of the competition between the increase in disparity with IBB concentration increase as  $MW_n$  decreases and the reduction in mobility with IBB concentration as  $MW_n$  increases. Blanco *et al.*<sup>29</sup> have observed a competing effect from mobility (from  $1/\eta$  of the mixture) and similarity (from the molecular weight difference  $\delta M$  of the  $n$ -alkanes in a binary  $n$ -alkane mixture) which may be related to the minimum for the  $D_T$  dependency on  $\delta M$  in equimolar  $nC_6$ - $nC_i$  mixtures. Fickian diffusion coefficients are dominated by mobility, but thermal diffusion coefficients are related to both mobility and similarity.

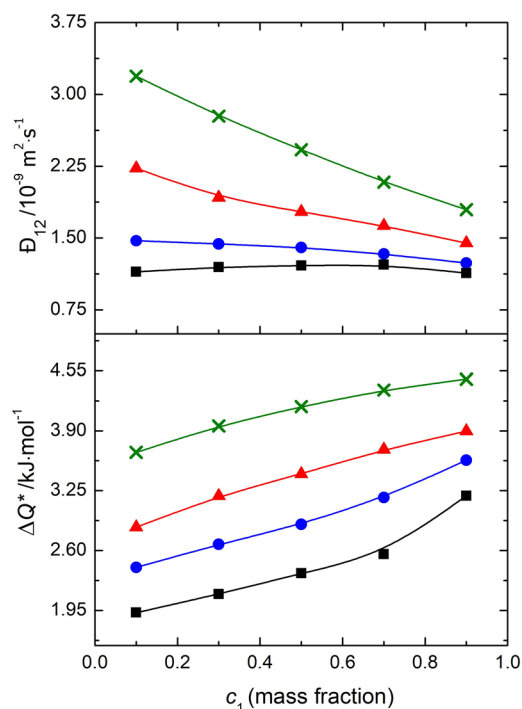


FIG. 11. Mobility ( $\mathcal{D}_{12}$ ) and disparity ( $\Delta Q^*$ ) vs isobutylbenzene (IBB) concentration in mass fraction ( $c_1$ ) at 25 °C and 1 atm for the IBB- $n$ -alkane ( $nC_i$ ) ( $i = 6, 8, 10, 12$ ) binary mixtures. Black squares: IBB- $nC_{12}$ ; blue circles: IBB- $nC_{10}$ ; red triangles: IBB- $nC_8$ ; and green crosses: IBB- $nC_6$ . Solid lines are tendency splines.

#### IV. CONCLUSIONS

We have measured the Fickian diffusion, thermal diffusion, and Soret coefficients of 4 binary mixtures of isobutylbenzene and an  $n$ -alkane ( $nC_6$ ,  $nC_8$ ,  $nC_{10}$  or  $nC_{12}$ ) at 5 concentrations (0.10–0.90 mass fractions), at 25 °C and 1 atm. Our measurements from the OBD setup are validated extensively. The Fickian diffusion and thermal diffusion coefficients of the IBB- $nC_6$ , IBB- $nC_8$ , and IBB- $nC_{10}$  mixtures are measured for the first time in the whole concentration range.

In this work, we show that the temperature contrast factor  $(\partial n/\partial T)_{P,c}$  for binary mixtures can be estimated using the laser deflection data in the OBD experiments. The accuracy of our method is the same as direct measurement by an interferometer with an error of the order of  $10^{-6}$ . The use of a robust stochastic optimization method is an integral part of our proposal.

We present an analysis of our measured  $D_{12}$  and  $D_T$  dependency on concentration (mass fraction of IBB) and normalized molecular weight ( $MW_n = MW_{nC_i}/MW_{IBB}$ ). Our analysis is based on mobility and similarity (or disparity, i.e., the inverse of similarity) of molecules. It is shown that solvent mobility can describe Fickian diffusion coefficients ( $D_{12}$ ), whereas both mobility and similarity should be invoked to describe thermal diffusion coefficients ( $D_T$ ). The mobility and similarity concepts are also used to examine the crossover point in the  $D_T$  vs  $MW_n$  plots. The crossover point is defined as the normalized molecular weight for which there is no concentration dependency of  $D_T$ . It is shown that the  $n$ -alkane chain

length drastically affects the  $D_{12}$  and  $D_T$  dependency on concentration. There is a decrease in  $D_T$  as concentration of IBB increases in the IBB- $nC_i$  mixtures for  $i = 6$  and 8. There is an increase in  $D_T$  with IBB concentration increase for the IBB- $nC_i$  mixtures for  $i = 10$  and 12.  $D_{12}$  dependency on concentration diminishes as  $n$ -alkane molecular size increases.

The effect of molecular size, shape, and concentration observed in Fickian and thermal diffusion coefficients discussed above may set the stage for future studies of mixtures containing aromatic components with large alkane branches and heteroatoms.

## ACKNOWLEDGMENTS

The authors thank CNPq (Conselho Nacional de Desenvolvimento Científico e Tecnológico—Brazil) for the fellowship granted through the Science Without Borders program (Programa Ciência Sem Fronteiras) during the period of November 2014 to October 2015. The authors also thank Reservoir Engineering Research Institute (RERI) that supported this work. We would like to thank

ATOMS Laboratory (Laboratory of Applied Thermodynamics and Molecular Simulation) in Federal University of Rio de Janeiro (Brazil) for the use of their cluster of computers in the calculations. We thank Professor Frederico Wanderley Tavares of the Federal University of Rio de Janeiro and Professor Juan Fernández de la Mora of Yale University for the help and facilitation of the work at Yale University.

## APPENDIX: CONTRAST FACTOR SENSITIVITY ANALYSIS

The sensitivity of Fickian diffusion, thermal diffusion, and Soret coefficients in the Optical Beam Deflection Technique on the contrast factors is discussed below.

Consider the IBB- $nC_6$  mixture. A  $\pm 5\%$  variation in  $(\partial n/\partial c_1)_{P,T}$  and  $(\partial n/\partial T)_{P,c}$  is considered separately (one single parameter per time). The coefficients  $D_{12}$ ,  $D_T$ , and  $S_T$  are determined using the procedure described in Sec. II. Figure 12 shows the effect.

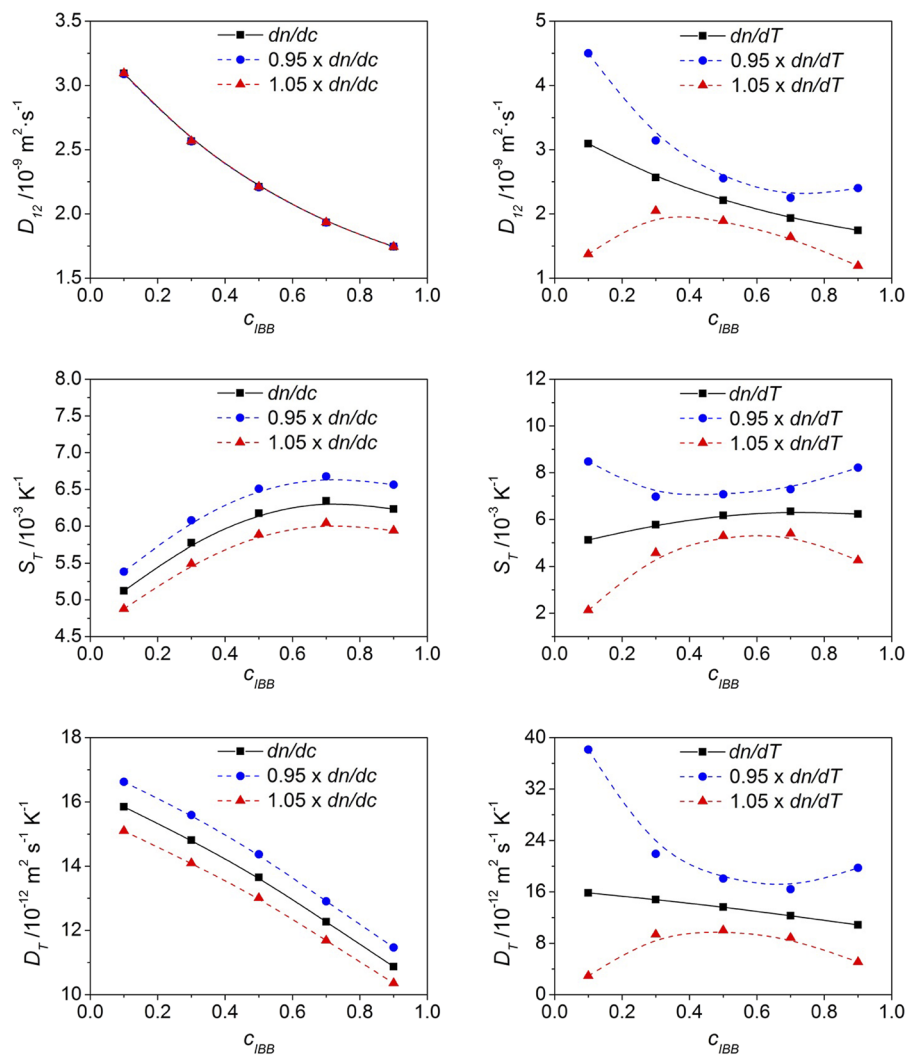


FIG. 12. Sensitivity of Fickian Diffusion ( $D_{12}$ ), thermal diffusion ( $D_T$ ), and Soret coefficients ( $S_T$ ) vs concentration of IBB in mass fraction to the concentration  $(\partial n/\partial c_1)_{P,T}$  and temperature  $(\partial n/\partial T)_{P,c}$  contrast factors.: IBB - $n$ -hexane( $nC_6$ ) mixture at 25 °C and 1 atm.



According to Fig. 12, the composition contrast factor  $(\partial n/\partial c_1)_{P,T}$  has an almost linear relation with  $D_T$  and  $S_T$ ; a 5% variation in  $(\partial n/\partial c_1)_{P,T}$  results in almost 5% variation in  $D_T$  and  $S_T$  for the entire range of concentrations. In  $D_{12}$ , a  $\pm 5\%$  variation in  $(\partial n/\partial c_1)_{P,T}$  has negligible influence.

There is a high dependency of the diffusion coefficients on accuracy of  $(\partial n/\partial T)_{P,c}$ , especially in the limits of concentration; a  $\pm 5\%$  variation in temperature contrast factor may result in  $-75\%$  to  $150\%$  variation in  $D_{12}$ ,  $D_T$ , and  $S_T$ .

## REFERENCES

- C. Ludwig, Sitzungsber. Akad. Wiss. Wien, Math.-Naturwiss. **20**, 539 (1856).
- C. Soret, C. R. Acad. Sci. **91**, 289 (1880).
- G. Wittko and W. Köhler, *Europhys. Lett.* **78**(4), 46007 (2007).
- D. A. de Mezquia, Z. Wang, E. Lapeira, M. Klein, S. Wiegand, and M. M. Bou-Ali, *Eur. Phys. J. E* **37**, 106 (2014).
- A. Leahy-Dios, "Experimental and theoretical investigation of Fickian and thermal diffusion coefficients in hydrocarbon mixtures," Ph.D. thesis, Yale University, 2008.
- S. R. de Groot and P. Mazur, *Non-Equilibrium Thermodynamics* (Dover Publications, New York, 1984).
- Y. Demirel, *Non-Equilibrium Thermodynamics: Transport and Rate Processes in Physical, Chemical and Biological Systems*, 2nd ed. (Elsevier, Amsterdam, 2007).
- A. Würger, *C. R. Mec.* **341**(4-5), 438 (2013).
- K. B. Haugen and A. Firoozabadi, *J. Phys. Chem. B* **110**(35), 17678 (2006).
- S. Wiegand, *J. Phys.: Condens. Matter* **16**(10), R357 (2004).
- J. K. Platten, *J. Appl. Mech.* **73**(1), 5 (2006).
- S. Srinivasan and M. Z. Saghir, *Int. J. Therm. Sci.* **50**(7), 1125 (2011).
- M. A. Rahman and M. Z. Saghir, *Int. J. Heat Mass Transfer* **73**, 693 (2014).
- W. Köhler and K. I. Morozov, *J. Non-Equilib. Thermodyn.* **41**(3), 151 (2016).
- J. K. Platten, M. M. Bou-Ali, P. Costesèque, J. F. Dutrieux, W. Köhler, C. Leppla, S. Wiegand, and G. Wittko, *Philos. Mag.* **83**(17-18), 1965 (2003).
- P. Costesèque and J. C. Loubet, *Philos. Mag.* **83**(17-18), 2017 (2003).
- M. M. Bou-Ali, J. J. Valencia, J. A. Madariaga, C. Santamaria, O. Encenarro, and J. F. Dutrieux, *Philos. Mag.* **83**(17-18), 2011 (2003).
- J. K. Platten, M. M. Bou-Ali, and J. F. Dutrieux, *Philos. Mag.* **83**(17-18), 2001 (2003).
- C. Leppla and S. Wiegand, *Philos. Mag.* **83**(17-18), 1989 (2003).
- G. Wittko and W. Köhler, *Philos. Mag.* **83**(17-18), 1973 (2003).
- M. Gebhardt, W. Köhler, A. Mialdun, V. Yasnou, and V. Shevtsova, *J. Chem. Phys.* **138**(11), 114503 (2013).
- J. Janca, V. Kaspárková, V. Halabalová, L. Simek, J. Ruzicka, and E. Barosová, *J. Chromatogr. B* **852**(1-2), 512 (2007).
- W. Köhler, C. Rosenauer, and P. Rossmanith, *Int. J. Thermophys.* **16**(1), 11 (1995).
- M. E. Schimpf and J. C. Giddings, *Macromolecules* **20**(7), 1561 (1987).
- F. Montel, J. Bickert, A. Lagisquet, and G. Galliero, *J. Pet. Sci. Eng.* **58**(3-4), 391 (2007).
- K. Ghorayeb and A. Firoozabadi, *SPE J.* **5**(2), 158 (2000).
- K. Ghorayeb, A. Firoozabadi, and T. Anraku, *SPE J.* **8**(2), 114 (2003).
- K. Ghorayeb, T. Anraku, and A. Firoozabadi, in Proceedings of SPE Asia Pacific Conference on Integrated Modelling for Asset Management, Yokohama, Japan, 25-26 April 2000.
- P. Blanco, M. M. Bou-Ali, J. K. Platten, P. Urteaga, J. A. Madariaga, and C. Santamaria, *J. Chem. Phys.* **129**(17), 174504 (2008).
- J. A. Madariaga, C. Santamaria, M. M. Bou-Ali, P. Urteaga, and D. A. de Mezquia, *J. Phys. Chem. B* **114**(20), 6937 (2010).
- D. A. de Mezquia, M. M. Bou-Ali, J. A. Madariaga, and C. Santamaria, *J. Chem. Phys.* **140**(8), 084503 (2014).
- A. Perronace, C. Leppla, F. Leroy, B. Rousseau, and S. Wiegand, *J. Chem. Phys.* **116**(9), 3718 (2002).
- F. A. Furtado, A. J. Silveira, C. R. A. Abreu, and F. W. Tavares, *Braz. J. Chem. Eng.* **32**(3), 683 (2015).
- P. Polyakov, J. Luettmer-Strathmann, and S. Wiegand, *J. Phys. Chem. B* **110**(51), 26215 (2006).
- S. M. Hashmi, S. Senthilnathan, and A. Firoozabadi, *J. Chem. Phys.* **145**(18), 184503 (2016).
- M. L. Larrañaga, M. M. Bou-Ali, E. Lapeira, I. Lizarraga, and C. Santamaria, *J. Chem. Phys.* **145**(13), 134503 (2016).
- S. Hartmann, G. Wittko, and W. Köhler, *Phys. Rev. Lett.* **109**(6), 065901 (2012).
- K. I. Morozov, *Phys. Rev. E* **79**(3), 031204 (2009).
- S. Hartmann, G. Wittko, F. Schook, W. Groß, F. Lindner, W. Köhler, and K. I. Morozov, *J. Chem. Phys.* **141**(13), 134503 (2014).
- K. J. Zhang, M. E. Briggs, R. W. Gammon, and J. V. Sengers, *J. Chem. Phys.* **104**(17), 6881 (1996).
- A. Königer, B. Meier, and W. Köhler, *Philos. Mag.* **89**(10), 907 (2009).
- A. Königer, H. Wunderlich, and W. Köhler, *J. Chem. Phys.* **132**(17), 174506 (2010).
- P. Kolodner, H. Willians, and C. Moe, *J. Chem. Phys.* **88**(10), 6512 (1988).
- A. J. Königer, "Optische untersuchung diffusiver transportvorgänge in mehrkomponentigen fluiden," Ph.D. thesis, Universität Bayreuth, 2012.
- J. F. Torres, A. Komiya, D. Henry, and S. Maruyama, *J. Chem. Phys.* **139**(7), 074203 (2013).
- D. T. J. Hurle and E. Jakeman, *J. Fluid Mech.* **47**(4), 667 (1971).
- G. Zimmermann and U. Müller, *Int. J. Heat Mass Transfer* **35**(9), 2245 (1992).
- B. E. Poling, J. M. Prausnitz, and J. P. O'Connell, *The Properties of Gases and Liquids*, 5th ed. (McGraw-Hill, 2001).
- C. L. Yawls, *Transport Properties of Chemicals and Hydrocarbons: Viscosity, Thermal Conductivity, and Diffusivity of Cl to Cl00 Organics and Ac to Zr Inorganics* (William Andrew, New York, 2009).
- R. R. Dreisbach, *Physical Properties of Chemical Compounds II*, 1st ed. (American Chemical Society, Washington, 1959).
- R. L. David, *CRC Handbook of Chemistry and Physics*, 90th ed. (CRC Press/Taylor and Francis, Boca Raton, FL, 2010).
- R. H. Perry, D. W. Green, and J. O. Maloney, *Perry's Chemical Engineers' Handbook*, 7th ed. (McGraw-Hill, New York, 1997).
- V. V. Sechenyh, J. C. Legros, and V. Shevtsova, *J. Chem. Thermodyn.* **43**(11), 1700 (2011).
- R. D. Camerini-Otero, R. M. Franklin, and L. A. Day, *Biochemistry* **13**(18), 3763 (1974).
- A. Becker, W. Köhler, and B. Müller, *Ber. Bunsen-Ges. Phys. Chem.* **99**(4), 600 (1995).
- J. Kennedy and R. Eberhart, in *Proceedings of the IEEE International Conference on Neural Networks* (IEEE, Perth, WA, Australia, 1995).
- M. Schwaab, E. C. Biscaia, Jr., J. L. Monteiro, and J. C. Pinto, *Chem. Eng. Sci.* **63**(6), 1542 (2008).
- M. Schwaab and J. C. Pinto, *Chem. Eng. Sci.* **62**(10), 2750 (2007).
- C. O. Ourique, E. C. Biscaia, Jr., and J. C. Pinto, *Comput. Chem. Eng.* **26**(12), 1783 (2002).
- L. R. Petzold, "A description of DASSL: A differential/algebraic system solver," in Proceedings of 10th IMACS World Congress, Canada, 1982.
- A. Leahy-Dios and A. Firoozabadi, *J. Phys. Chem. B* **111**(1), 191 (2007).
- A. Leahy-Dios, L. Zhuo, and A. Firoozabadi, *J. Phys. Chem. B* **112**(20), 6442 (2008).
- H. J. V. Tyrrel and K. R. Harris, *Diffusion in Liquids: A Theoretical and Experimental Study* (Butterworth, London, 1984).
- F. Reif, *Fundamentals of Statistical and Thermal Physics* (Waveland Press, USA, 2009).
- A. L. Van Geet and A. W. Adamson, *Ind. Eng. Chem.* **57**(7), 62 (1965).
- L. S. Darken, *Trans. Am. Inst. Min. Metall. Eng.* **175**, 184 (1948).
- R. K. Ghai, H. Ertl, and F. A. L. Dullien, *AIChE J.* **19**(5), 881 (1973).
- A. Vignes, *Ind. Eng. Chem. Fundam.* **5**(2), 189 (1966).
- H. Kramers and J. J. Broeder, *Anal. Chim. Acta* **2**, 687 (1948).
- R. Kita, P. Polyakov, and S. Wiegand, *Macromolecules* **40**(5), 1638 (2007).

- <sup>71</sup>J. Demichowicz-Pigoniowa, M. Mitchell, and H. J. V. J. Tyrrell, *J. Chem. Soc. A* **2**(0), 307 (1971).
- <sup>72</sup>S. Srinivasan and M. Z. Saghir, *Thermal Diffusion in Multicomponent Mixtures: Thermodynamic, Algebraic and Neuro-Computing Models*, 1st ed. (Springer, New York, 2013).
- <sup>73</sup>E. L. Dougherty and H. G. Drickamer, *J. Chem. Phys.* **23**(2), 295 (1955).
- <sup>74</sup>K. G. Denbigh, *Trans. Faraday Soc.* **48**, 1 (1952).
- <sup>75</sup>A. Firoozabadi, K. Ghorayeb, and K. Shukla, *AIChE J.* **46**(5), 892 (2000).
- <sup>76</sup>K. Shukla and A. Firoozabadi, *Ind. Eng. Chem. Res.* **37**(8), 3331 (1998).
- <sup>77</sup>R. Taylor and R. Krishna, *Multicomponent Mass Transfer*, 1st ed. (Wiley-Interscience, New York, 1993).
- <sup>78</sup>A. Firoozabadi, *Thermodynamics and Applications in Hydrocarbon Energy Production*, 1st ed. (McGraw-Hill, 2016).
- <sup>79</sup>D. Peng and D. B. Robinson, *Ind. Eng. Chem. Fundam.* **15**(1), 59 (1976).
- <sup>80</sup>W. B. Li, P. N. Segrè, R. W. Gammon, J. V. Sengers, and M. Lamvik, *J. Chem. Phys.* **101**(6), 5058 (1994).
- <sup>81</sup>R. K. Ghai and F. A. L. Dullien, *J. Phys. Chem.* **78**(22), 2283 (1974).
- <sup>82</sup>W. Köhler and B. Müller, *J. Chem. Phys.* **103**(10), 4367 (1995).
- <sup>83</sup>M. M. Bou-Ali, O. Encenarro, J. A. Madariaga, C. M. Santamaría, and J. J. Valencia, *J. Phys.: Condens. Matter* **10**(15), 3321 (1998).
- <sup>84</sup>P. Blanco, M. M. Bou-Ali, J. K. Platten, D. A. de Mezquia, J. A. Madariaga, and C. Santamaría, *J. Chem. Phys.* **132**(11), 114506 (2010).
- <sup>85</sup>M. A. Rahman, "Experimental measurement of Soret coefficient of binary hydrocarbon mixtures," Ph.D. thesis, Ryerson University, 2013.
- <sup>86</sup>D. A. De Mezquia, M. M. Bou-Ali, M. Larrañaga, J. A. Madariaga, and C. Santamaría, *J. Phys. Chem. B* **116**(9), 2814 (2012).
- <sup>87</sup>K. R. Harris, J. J. Alexander, T. Goscinska, R. Malhotra, L. A. Woolf, and J. H. Dymond, *Mol. Phys.* **78**(1), 235 (1993).
- <sup>88</sup>M. V. Rathnam, K. Jain, and M. S. S. Kumar, *J. Chem. Eng. Data* **55**(4), 1722 (2010).
- <sup>89</sup>M. V. Rathnam, K. Jain, S. Mankumare, and M. S. S. Kumar, *J. Chem. Eng. Data* **55**(9), 3929 (2010).
- <sup>90</sup>M. V. Rathnam, R. T. Sayed, K. R. Bhanushali, and M. S. S. Kumar, *J. Mol. Liq.* **166**, 9 (2012).
- <sup>91</sup>P. Polyakov and S. Wiegand, *Thermal Diffusion: Basics and Applications (IMT7)* (Mondragon Unibertsitatea, Mondragon, 2006), pp. 399–407.
- <sup>92</sup>L. Grunberg and A. H. Nissan, *Nature* **164**, 799 (1949).
- <sup>93</sup>J. D. Isdale, J. C. MacGillivray, and G. Cartwright, "Prediction of viscosity of organic liquid mixtures by a group contribution method," National Engineering Laboratory Report, East Kilbride, Glasgow, Scotland, 1985.